# Neurocalcin Delta Suppression Protects against Spinal Muscular Atrophy in Humans and across Species by Restoring Impaired Endocytosis

Markus Riessland,[1,2,3,13,14] Anna Kaczmarek,[1,2,3,13] Svenja Schneider,[1,2,3,13] Kathryn J. Swoboda,[4] Heiko Löhr,[5,7] Cathleen Bradler,[6,7] Vanessa Grysko,[1,2,3] Maria Dimitriadi,[8,15] Seyyedmohsen Hosseinibarkooie,[1,2,3] Laura Torres-Benito,[1,2,3] Miriam Peters,[1,2,3] Aaradhita Upadhyay,[1,2,3] Nasim Biglari,[1,2,3] Sandra Kröber,[1,2,3] Irmgard Hölker,[1,2,3] Lutz Garbes,[1,2,3] Christian Gilissen,[9] Alexander Hoischen,[9] Gudrun Nürnberg,[7,10] Peter Nürnberg,[7,10] Michael Walter,[11] Frank Rigo,[12] C. Frank Bennett,[12] Min Jeong Kye,[1,2] Anne C. Hart,[8] Matthias Hammerschmidt,[2,5,7] Peter Kloppenburg,[6,7] and Brunhilde Wirth[1,2,3,*]

Homozygous *SMN1* loss causes spinal muscular atrophy (SMA), the most common lethal genetic childhood motor neuron disease. *SMN1* encodes SMN, a ubiquitous housekeeping protein, which makes the primarily motor neuron-specific phenotype rather unexpected. SMA-affected individuals harbor low SMN expression from one to six *SMN2* copies, which is insufficient to functionally compensate for *SMN1* loss. However, rarely individuals with homozygous absence of *SMN1* and only three to four *SMN2* copies are fully asymptomatic, suggesting protection through genetic modifier(s). Previously, we identified plastin 3 (PLS3) overexpression as an SMA protective modifier in humans and showed that SMN deficit impairs endocytosis, which is rescued by elevated PLS3 levels. Here, we identify reduction of the neuronal calcium sensor Neurocalcin delta (NCALD) as a protective SMA modifier in five asymptomatic *SMN1*-deleted individuals carrying only four *SMN2* copies. We demonstrate that NCALD is a $Ca^{2+}$-dependent negative regulator of endocytosis, as NCALD knockdown improves endocytosis in SMA models and ameliorates pharmacologically induced endocytosis defects in zebrafish. Importantly, NCALD knockdown effectively ameliorates SMA-associated pathological defects across species, including worm, zebrafish, and mouse. In conclusion, our study identifies a previously unknown protective SMA modifier in humans, demonstrates modifier impact in three different SMA animal models, and suggests a potential combinatorial therapeutic strategy to efficiently treat SMA. Since both protective modifiers restore endocytosis, our results confirm that endocytosis is a major cellular mechanism perturbed in SMA and emphasize the power of protective modifiers for understanding disease mechanism and developing therapies.

## Introduction

In monogenic disorders, genetic modifiers can influence disease-causing mechanisms resulting in incomplete penetrance.[1] Identification of such modifiers is of utmost relevance since they can uncover regulatory networks and pathological mechanisms, as well as allow identification of therapeutic pathways. For recessive disorders, full protection through modifiers is extremely rare, making their identification highly challenging.

Spinal muscular atrophy (SMA), a motor neuron disease, is one of the most common and devastating autosomal-recessive disorders, for which no treatment is available yet. However, various clinical trials using antisense oligonucleotides (ASOs), small molecules, or gene therapy show highly promising ameliorations.[2] Most SMA individuals show homozygous absence of exon 7 of survival motor neuron 1 (*SMN1* [MIM: 600354]),[3] allowing easy and efficient genetic testing.[4] *SMN1* encodes SMN, a housekeeping protein involved in snRNP biogenesis and splicing, microRNA biogenesis, transcription and translation regulation, and others;[5–8] full absence of SMN causes embryonic lethality.[9] Only humans have an almost identical copy, *SMN2* (MIM: 601627), but this produces only ~10% correctly spliced full-length transcript and protein, due to a single silent mutation affecting an exonic splicing enhancer and creating a new splice silencer.[10–12] In SMA-affected individuals, *SMN2* is the only source of SMN, so its copy number (between 1 and 6) determines SMA severity.[13] In type 1 SMA (SMA1 [MIM: 253300]), the severe and most common form (60%), the majority of individuals carry two *SMN2* copies and die within the first 2 years of life. Most type 2 SMA (SMA2 [MIM: 253550])-affected individuals carry three *SMN2* copies

[1]Institute of Human Genetics, University of Cologne, 50931 Cologne, Germany; [2]Center for Molecular Medicine Cologne, University of Cologne, 50931 Cologne, Germany; [3]Institute for Genetics, University of Cologne, 50674 Cologne, Germany; [4]MassGeneral Hospital for Children, Boston, MA 02115, USA; [5]Institute for Zoology - Developmental Biology, University of Cologne, 50674 Cologne, Germany; [6]Institute for Zoology - Neurophysiology University of Cologne, 50674 Cologne, Germany; [7]Excellence Cluster on Cellular Stress Responses in Aging Associated Diseases (CECAD), University of Cologne, 50931 Cologne, Germany; [8]Department of Neuroscience, Brown University, Providence, RI 02912, USA; [9]Department of Human Genetics, Donders Centre for Neuroscience, Radboud University Medical Center, 6525 Nijmegen, the Netherlands; [10]Center for Genomics Cologne, University of Cologne, 50931 Cologne, Germany; [11]Institute of Medical Genetics, University of Tübingen, 72076 Tübingen, Germany; [12]IONIS Pharmaceuticals, Carlsbad, CA 92008, USA
[13]These authors contributed equally to this work
[14]Present address: Laboratory of Molecular and Cellular Neuroscience, The Rockefeller University, New York, NY 10065, USA
[15]Present address: Department of Biological and Environmental Sciences, University of Hertfordshire, Hatfield AL10 9AB, UK
*Correspondence: brunhilde.wirth@uk-koeln.de
http://dx.doi.org/10.1016/j.ajhg.2017.01.005.

and are never able to walk. In type 3 SMA (SMA3 [MIM: 253400]), the mild form, most individuals carry four *SMN2* copies and are able to walk, but often become wheelchair bound.[14]

Despite the important housekeeping function of SMN, reduced levels primarily cause spinal motor neuron (MN) dysfunction in all types of SMA.[14] Thus, MN loss, impaired maturation and maintenance of neuromuscular junctions (NMJs), and decreased proprioceptive inputs on MN soma are hallmarks of SMA.[15–17] Nonetheless, dramatic reduction of SMN below a certain threshold, as seen in severely affected SMA individuals or animal models, compromises almost every organ and many different cellular processes, which is in line with the essential function of SMN in all cell types.[18,19] Therefore, we reasoned that the search for the main cellular pathway specifically driving MN dysfunction has to be carried out in mildly affected SMA individuals, in whom only motor neuron function is impaired and moreover, that protective modifiers identified in these individuals may reveal the critical underlying cellular mechanism.

To do so, we took advantage of very rarely occurring SMA-discordant families, in which relatives of SMA-affected individuals carry a homozygous *SMN1* deletion together with three or four *SMN2* copies but are clinically asymptomatic.[20–23] In seven of these families, we previously identified the $Ca^{2+}$-dependent protein Plastin 3 (PLS3) as a protective modifier.[24,25] PLS3 overexpression (OE) rescues SMA across species and is specifically upregulated in MNs of asymptomatic individuals produced from induced pluripotent stem cells.[24,26–29] Moreover, PLS3 together with the second modifier found in this study pointed us toward endocytosis as the key disturbed cellular mechanism in SMA.[29]

Here, we report the identification of Neurocalcin delta (*NCALD* [MIM: 606722]), which encodes a neuronal $Ca^{2+}$ sensor protein, as an SMA-protective modifier in humans. We show that NCALD acts as a negative regulator of endocytosis, which is in contrast to PLS3 acting as its positive regulator. We show $Ca^{2+}$-dependent interaction of NCALD with clathrin, a protein essential in endocytic vesicles coating. We demonstrate that low SMN levels reduce voltage-dependent $Ca^{2+}$ influx and that NCALD binds clathrin at low $Ca^{2+}$ levels, thereby acting as a $Ca^{2+}$-sensitive inhibitor of endocytosis. Our results, obtained from multiple in vitro and in vivo systems, show that NCALD suppression reestablishes synaptic function, most likely by restoring endocytosis. Most importantly, we prove that NCALD knockdown (KD) in various SMA animal models ameliorates major functional SMA disturbances, such as motor axon development in zebrafish or MN circuitry and presynaptic function of neuromuscular junction (NMJ) in mice. Moreover, we introduce a mild SMA mouse model generated by combined low-dose SMN-ASO treatment and heterozygous loss of *Ncald* that show restored motoric function. Our data support the notion that genetic modifiers reveal additional valuable treatment options, beyond existing therapies.

## Material and Methods

### Individuals' DNA, Fibroblast Cell Lines, and Lymphoblastoid Cell Lines

Informed written consent was obtained from each subject or their legal guardians for all biological samples according to the Declaration of Helsinki. The study has been approved by the Ethical Committee of University of Cologne (04-138). Human fibroblast and EBV-transformed lymphoblastoid cell lines (LBs) from SMA-affected individuals, carriers, and asymptomatic *SMN1*-deleted individuals used in this work are listed in Table S1. DNA was extracted from EDTA blood samples, primary fibroblast cell lines, and LBs using standard protocols. *SMN1* and *SMN2* copy number were determined by qRT-PCR or MLPA lysis (MRC Holland) as described.[30] For haplotype analysis, polymorphic markers Ag1-CA (D5S1556), C212 (D5F149S1/S2), VS19A (D5S435), and MIT-I105 (D5S351) were analyzed as described.[31] *SMN2* coding region was sequenced in qRT-PCR products obtained from LB-isolated RNA as described.[32] *PLS3* expression was analyzed as described.[24] All cell lines used were tested for mycoplasma contamination.

### Genome-wide Linkage Analysis

Genome-wide scan was performed in 14 individuals of the Utah family using Affymetrix GeneChip Human Mapping 10K Array 2.0, which comprises 10,024 SNPs with a mean intermarker distance of 258 kb, equivalent to 0.36 cM (Affymetrix). Parametric linkage analysis was performed by ALLEGRO program[33] assuming autosomal-dominant inheritance with full penetrance and 0.0001 disease allele frequency. Haplotypes were reconstructed with ALLEGRO and presented graphically with HaploPainter.[34] All data handling was performed using the graphical user interface ALOHOMORA.[35]

### Transcriptome Analysis

For expression profiling, 400 ng total RNA were amplified and biotinylated using Illumina TotalPrepTMRNA Amplification Kits (Ambion) according to manufacturer's protocol. Human HT-12v3 bead arrays (Illumina) were hybridized with 750 ng cRNA for 18 hr at 58°C according to Illumina Whole-Genome Gene Expression with IntelliHyb SealSystem Manual. Arrays were washed with E1BC buffer, High-Temp Wash Buffer, and 100% ethanol, stained with streptavidine-Cy3, and washed with E1BC buffer. Fluorescence intensities were recorded on BeadArray Reader GX (Illumina). Average signal intensities without background correction[36] were performed with BeadStudio3.1 (Illumina). All data analysis steps were performed in the statistical environment R (v.2.10-0) with several bioconductor packages (v.2.6.1). Signal intensities were normalized with VSN (variance stabilizing and normalization quantification method[37]) and non-informative probes were removed based on p values. Signals were averaged for individual subgroups and a linear model was designed capturing the influence of the asymptomatic group on gene expression levels.[38] Differences between subgroups were extracted as contrasts and analyzed with the moderated F-test (empirical Bayes method) including a correction step for multiple testing with 5%-FDR-based method.[39] To attribute significant regulations to individual contrasts, a decision matrix was generated based on the function "decide tests" within the "limma" package, where significant up- or downregulations are represented by values of 1 or −1, respectively.

## Targeted Resequencing

To identify a potential variant regulating differential *NCALD* expression, complete *NCALD* locus ± 1 Mb (chr8: 101,505,353–104,404,346) was deep-sequenced from gDNA of family members II-1, III-1, III-4, III-8, and IV-3 at Radboud University Medical Center Nijmegen using a 5500xl sequencing instrument (Life Technologies). ~3 Mb genomic DNA from chromosome 8 were captured using a 385K NimbleGen SequenceCapture Array (Roche).

On average, we obtained 2.7 Gb of mappable sequence data/individual. Reads were mapped to the hg19 reference genome with Life Technologies BioScope software 1.3. On average, 94% of bases originated from the target region (mean 544-fold coverage). 99.8% of the targeted region was covered ≥20 times. Single-nucleotide variants were subsequently high-stringency called by the DiBayes algorithm. Small insertions and deletions were detected using the Small IndelTool. Variants were annotated using an in-house analysis pipeline.

## Zebrafish Experiments

All experiments were performed with the transgenic line *tg(mnx1-GFP)*$^{ml2TG\ 40}$ and approved by the local animal protection committee (LANUV NRW; reference number 84-02.04.2012.A251).

### *Zebrafish Injection and Analysis*

Morpholinos (MO) were designed against the translational start codons of respective genes (Gene Tools, LLC). *smn*-MO: 5′-CGA CATCTTCTGCACCATTGGC-3′; *ncaldb*-MO: 5′-GGAGCTTGCTG TTTTGTTTTCCCAT-3′; control-MO: 5′-CCTCTTACCTCAGTTA CAATTTATA-3′. For *NCALD* mRNA injections, human *NCALD* cDNA was cloned into pCS2+ mRNA expression vector and transcribed in vitro using mMESSAGE mMACHINE SP6 Transcription Kit (Ambion) according to manufacturer's protocol. Embryos from TL/EK wild-type and TL/EK-*hb9-GFP*[40] crossings were used to visualize the MN phenotype. Embryos were injected with the respective dose of MOs or mRNA in aqueous solution containing 0.05% PhenolRed and 0.05% Rhodamine-Dextran (Sigma). 6 hr after injection, embryos were sorted according to homogeneity of the rhodamine fluorescence signal.

### *Immunohistochemistry for Motor Axon Quantification*

34 hpf zebrafish were manually dechorionated, fixed in 4% PFA-PBS, and permeabilized by collagenase digest of the whole animal. To visualize the primary motor axons, zebrafish were incubated at 4°C overnight in PBS-T/1%DMSO/10%FCS containing znp-1 antibody (AB2315626, Hybridoma Bank) and stained in PBS-T/1%DMSO/10%FCS containing donkey anti-mouse secondary antibody labeled with AlexaFluor488 (Invitrogen) after all-day washing in PBS-T/1%FCS/1%BSA (changing solution hourly) and stored in 80% glycerol/20% PBS in the dark at 4°C or embedded in low-melting agarose microslides for microscopy analysis. The structure of first ten motor axons posterior to the yolk was analyzed, rated as: (1) normal, (2) truncated (truncation ventral from midline), (3) severely truncated (shorter than midline), (4) branched I (branching ventral from midline), (5) branched II (branching at midline), or (6) branched III (branching dorsal from midline).

### *Western Blot Analysis of Zebrafish*

48 hpf dechorionated embryos were gently spun down, sacrificed by incubation on ice, and lysed in RIPA buffer (Sigma) containing protease inhibitors (Complete Mini, Roche). The following primary antibodies were used for overnight incubation: anti-beta-actin (zebrafish) (553399, Anaspec), anti-SMN (MANSMA7, Hybridoma Bank; 610646, BD Biosciences), and anti-NCALD (12925-1-AP, Proteintech). Signal detection was performed as described above.

### *Transmission Electron Microscopy of Zebrafish*

48 hpf zebrafish were fixed in 4% PFA for 30 min and postfixed in 0.6% glutaraldehyde for another day. Samples were prepared and embedded in resin as previously described.[27] The thickness of semi-thin and ultra-thin sections was 0.5 and 0.1 mm, respectively. For immunogold stainings, pre-stained sections were blocked, incubated with primary antibodies (anti-clathrin [ab273, Abcam], anti-NCALD), washed in PBS, and stained with gold-labeled secondary antibodies (donkey-anti-mouse 6 nm gold [ab39616, Abcam], goat-anti-rabbit 20 nm gold [ab27237, Abcam]). Image acquisition was performed with TEM CM10 (Philips) microscope, Orius SC200W 1 Gatan camera, and the Digital Micrograph software.

### *Motor Behavior Analysis of Zebrafish*

30 zebrafish treated with respective MOs were placed in 10 cm petri dish containing embryo medium. To trigger a swimming response, zebrafish were stimulated with an electrical impulse (60V; delay: 60 ms, duration: 4 ms, frequency: 6 pps [SD9 Stimulator]). Swimming behavior was recorded with 120 frames/s using a high-speed camera (FC-100, Casio). Swimming velocity and distance were analyzed using LoliTrack software (Loligo Systems).

### *Endocytosis Inhibitor Treatment*

Dynasore (dynamin inhibitor) and Pitstop2 (clathrin inhibitor) (Abcam) were dissolved as stock solutions (50 mM) in DMSO. Zebrafish were dechorionated and incubated with the respective inhibitors in the medium starting at 16 hpf at 28°C on a rocking platform (20 rpm) until fixed in 4% PBS-PFA at 34 hpf. Subsequent zebrafish immunohistochemistry was performed as described above.

### *Electrophysiology*

72 hpf zebrafish (control, *smn*-, *ncald*-, and *smn*+*ncald*-morphants) were anesthetized with 0.02% tricaine (in saline; Sigma) for 1–2 min and rinsed with saline containing (in mM): 134 NaCl, 2.9 KCl, 2.1 $CaCl_2$, 1.2 $MgCl_2$, 10 HEPES, 10 glucose adjusted to pH 7.8. Zebrafish were decapitated and pinned under saline in a Sylgard-coated (Dow Corning) recording chamber (~3 mL volume). Skin was removed using a tungsten pin and forceps; preparation was incubated in 3M formamide (in saline; Carl Roth) for 2 min to prevent muscle contractions. After rinsing the preparation, the superficial layer of ventral slow muscle cells was removed by scratching with a tungsten pin to expose deeper fast skeletal muscle cells and remaining superficial slow muscles were removed with a low-resistance pipette (~2 MΩ). The preparation was continuously superfused with saline at a flow rate of ~2 $mL/min^{-1}$. Experiments were carried out at ~24°C. Muscle cells were visualized with a fixed-stage upright microscope (Zeiss Axio Examiner, Zeiss), using a 40× water immersion objective (Zeiss) with infrared-differential interference contrast and fluorescence optics. Fast muscle cells were identified by their orientation to the spinal cord and ability to generate action potentials.

## *Caenorhabditis elegans* Experiments

Strains used were as follows: LM99 *smn-1(ok355)I/hT2(I;III)*,[41] HA1981 *+/hT2(I;III)*, HA2530 *+/hT2(I;III);ncs-1(qa401)X*, HA2531 *smn-1(ok355)I/hT2(I;III);ncs-1(qa401)X*, HA2599 *+/hT2(I;III);uIs72*, and HA2623 *smn-1(ok355)I/hT2(I;III);uIs72* were maintained at 20°C under standard conditions. *+/hT2* strains were used as control for genetic background; RNAi studies were undertaken in a

sensitized background (transgene *uIs72*) expressing the SID-1 dsRNA channel in neurons.[42]

#### C. elegans *Pharyngeal Pumping*

Pharyngeal grinder movement in any axis was scored as a pumping event. Average pumping rates (±SEM) were combined from at least three independent trials (n ≥ 25 animals in total). For RNAi knockdown, animals were reared for two generations (F2) on either control vector L4440 or C44C1.3/*ncs-1(RNAi)* in HT115. *ncs-1* RNAi clone contains genomic DNA amplified by primers 5′-AAATCGTCTAGCTGTAGTGTCGC-3′ and 5′-TTGTGC TCCCTACACTTTGTTTT-3′ inserted into L4440. Clone was verified by sequencing.

## Mouse Experiments

All mouse experiments were approved by LANUV NRW (reference number 9.93.2.10.31.07.186 and 84-02.04.2014.A 126). The Taiwanese SMA mice (FVB.Cg-Tg(SMN2)2Hung Smn1tm1Hung/J, Stock Number 005058) and heterozygous *Ncald*$^{ko/wt}$ mice (Bl6N(Cg)-*Ncald*$^{tm1.1(KOMP)Vlcg}$/J, Stock Number 018575) were purchased from Jackson Laboratory. The severe SMA (*Smn*$^{ko/ko}$; *SMN2*$^{tg/0}$) mice and the corresponding heterozygous *Smn* (HET [*Smn*$^{kowt-}$; *SMN2*$^{tg/0}$]) mice were produced as previously described.[9,43] The breeding scheme and genotypes for SMA-*Ncald*$^{ko/wt}$ and HET-*Ncald*$^{ko/wt}$ mice are similar to SMA+ASO-treated mice (Figure 5A), except that all animals were on congenic C57BL/6N and untreated.

Primers used for mouse genotyping are as follows: mmu *Smn*KOfw: 5′-ATAACACCACCACTCTTACTC-3′; mmu *Smn*KOrev1: 5′-AGCCTGAAGAACGAGATCAGC-3′; mmu *Smn*KOrev2: 5′-TAG CCGTGATGCCATTGTCA-3′; hsa *SMN2*fw: 5′-CGAATCACTTGAG GGCAGGAGTTTG-3′; hsa *SMN2*rev 5′-AACTGGTGGACATGGC TGTTCATTG-3′; mmu *Ncald*KOfw: 5′-CGGTCGCTACCATTAC-3′; mmu *Ncald*KOrev: 5′-GCATGTGTGACAACAG-3′.

A mild SMA mouse model was produced by suboptimal subcutaneous injection of severe SMA mice (50% FVB/N: 50% C57BL6/N) on P1 with 30 μg of SMN-ASO (IONIS Phamaceuticals) using a MICROLITER syringe (Hamilton). The SMN-ASO was diluted as previously described.[19] SMA-*Ncald*$^{ko/wt}$+ASO and HET-*Ncald*$^{ko/wt}$+ASO were produced using the breeding scheme in Figure 5A. Unless stated otherwise, all mouse experiments were performed blinded for genotype and treatment.

#### *Mouse Motoric Tests*

Righting reflex test was performed as previously described.[44] Righting time scores were evaluated as followed: 0–2 s, 1; 3–4 s, 2; 5–6 s, 3; 7–8 s, 4; 9–10 s, 5; ≥11 s, 6. Muscle strength was assessed in P73 SMN-ASO injected mixed$_{50}$ background mice by the animal's grasp of a horizontal metal bar mounted to a high-precision force sensor (Grip strength meter, TSE Systems). Muscle force was recorded in pounds and converted to Newton [N].

#### *Quantification of Proprioceptive Inputs*

Analysis of proprioceptive input on MN soma was performed as described.[29] The spinal cord was dissected from euthanized mice and fixed in 4% PFA overnight. The lumbar L4-L5 region was rinsed in PBS, embedded in tissue freezing medium (Jung) after cryoprotection (first day: 20% sucrose, second day: 30% sucrose), and sliced into 100 μm sections (cryostat, Leica). Samples were permeabilized, blocked in PBS/4% BSA/1% Triton/PBS for 1 hr, and incubated with anti-CHAT (Choline acetyltransferase, a MN-specific marker) (AB144P, Millipore) and anti-VGLUT1 (Vesicular glutamate transporter 1 or SLC17A, an excitatory neurotransmitter used for proprioceptive inputs) (135303, Synaptic Systems) antibodies overnight. Samples were washed and incubated with secondary antibodies (donkey anti-rabbit AlexaFluor488, donkey anti-goat AlexaFluor568) and mounted in Mowiol. Images were taken in Z stacks of 30–60 slices of 0.3 μm interval. Proprioceptive input numbers on MN and MN soma size were quantified using the ImageJ software.

#### *Quantification of NMJ Size and Maturity*

The transversus abdominis (TVA) muscle was prepared at the indicated time points and fixed in 4% PFA for 20 min. TVA was stained with anti-NF-M (Neurofilament M, NEFM, used as neuronal axon and dendritic marker [Hybridoma-Bank]) and with secondary goat-anti mouse AlexaFluor488 and Bungarotoxin (both Invitrogen, labeled with AlexaFluor555). Surface area of Bungarotoxin-positive post-synapse was measured by ImageJ with threshold set to the method established by Li. NMJ immaturity index was analyzed as described previously:[45] NMJs exhibiting ≥3 perforations were evaluated as mature, NMJs with <3 perforations as immature.

#### *FM1-43 Endocytic Uptake at NMJ under Electrical Stimulation*

FM1-43 endocytic uptake at NMJ under electrical stimulation was undertaken as recently described.[29] Three animals per genotype and stimulation set were used. Imaging was performed as described above. All imaging processes and analyses were performed double-blinded. Images were analyzed with ImageJ using a macro setting and Li threshold method applied to the postsynaptic terminals to delineate the area of interest in the presynaptic site.

#### *Microscopy*

Unless indicated otherwise, all microscopic experiments were performed with a fully motorized fluorescence microscope AxioImager M2 (Zeiss) equipped with an ApoTome. All quantitative measurements were performed using Zen software (Zeiss) and ImageJ and evaluated with indicated statistical packages.

#### *Primary Motor Neuron Culture*

Spinal cords were dissected from E13.5 mouse embryos.[9] Neurons were singularized with trypsin (Worthington) and DNase (Sigma), sieved, plated on poly-D-lysine/laminin (Sigma)-coated coverslips, and cultured in neurobasal medium with B27 supplement, 2 mM L-glutamine, 1× pen-strep (Invitrogen) containing 50 ng/μL BDNF, 50 ng/μL GCNF, and 50 ng/μL CNTF (Peprotech) at 37°C in a humidified incubator with 5% $CO_2$.

## Cell Culture Experiments

#### *Quantitative RT-PCR*

RNA was extracted from cell lines using RNeasy kit (QIAGEN). 150 ng RNA was reversely transcribed to cDNA (Quantitect Reverse Transcription Kit, QIAGEN). For *NCALD* cDNA measurements, 9 ng cDNA was used for RT-PCR (LightCycler, Roche). RT-PCR was performed in triplicates according to manufacturer's protocol (annealing temperature 68°C, *NCALD* cDNA primers: 5′-GGA ATGCCCAGAGCCCCAGTGT-3′; 5′-GCCCCAACCCCCGAGTCTT ACG-3′). Standard curve-based absolute transcript quantification was performed using Excel (Microsoft). For statistical evaluation, the Student's t test was applied. For quantitative measurements of *SMN* and *PLS3*, previously described protocols were used.[24]

#### *siRNA-Mediated RNA Knockdown*

For all siRNA experiments, NSC34 (CLU140)[32] and PC12[46] cells were transfected with Dharmafect1 (Thermo Scientific) according to manufacturer's protocol. siTOX (Dharmacon) and AllStars Negative Control (QIAGEN) siRNA were used as controls. siRNAs sequences: mmu-*Smn:* 5′-AAGAAGGAAAGTGCTCACA

TA-3′; mmu-*Ncald* 5′-CAGGTGATTCACCCATTATAA-3′; rn-*Smn* 5′-CCCGACCTGTGAAGTAGCTAA-3′; rn-*Ncald* 5′- AGAGACTTC CTAGCAATTTAA-3. After incubation, cells were harvested for protein isolation or imaging. Every experiment was performed at least in triplicates.

#### *Transient Overexpression*

Human *NCALD* cDNA was cloned into pcDNA3.1/CT-GFP TOPO using primers NCALD-FWD 5′-ATGGGGAAACAGAACAGCAA G-3′ and NCALD-REV 5′-GAACTGGCCGGCACTGCTC-3′ (IDT) and manufacturer's protocol (Invitrogen). To overexpress human NCALD-GFP, NSC34 cells were transfected with Dharmafect1 according to manufacturer's protocol.

#### *Western Blot Analysis*

Cells were lysed on ice in RIPA buffer (Sigma) containing protease inhibitors (Complete Mini, Roche). The following primary antibodies were used: anti-ACTB (actin, beta), used as control for equal loading (A5316, Sigma), anti-SMN (MANSMA7, Hybridoma Bank; 610646, BD Biosciences), anti-NCALD (12925-1-AP, Proteintech), and anti-CLTC (clathrin heavy chain) (C1860, Sigma). Signal was detected with HRP conjugated-secondary antibodies and Chemiluminescence reagent (Thermo Scientific) according to manufacturer's protocol.

#### *NCALD Co-immunoprecipitation*

NSC34 cells transiently transfected with pcDNA/FLAG-His-NCALD or control vector were lysed in the following buffer: 50 mM Tris/HCl, 5% (w/v) glycerol, 270 mM sucrose, 0.5%(v/v) Tween 20, 0.1%(v/v) β-mercaptoethanol (pH 7.5), with protease inhibitor cocktail (Complete Mini, EDTA-free, Roche). Immunoprecipitations were performed in 1 mM EGTA/1 mM EDTA or in the presence of 100 μM free $Ca^{2+}$. Cell lysates were immunoprecipitated with FLAG-M2 affinity beads (Sigma) under gentle agitation overnight at 4°C. Bound proteins were eluted in laemmli buffer (240 mM Tris-HCl [pH 6.8], 6% SDS, 30% (v/v) glycerol, 0.06% bromophenol blue (w/v), 16%(v/v) β-mercaptoethanol) and analyzed by western blots as described above.

#### *Immunocytochemistry*

Cells were cultured on laminin-coated coverslips, washed with PBS, fixed in 4% PFA/4% sucrose (AppliChem), permeabilized in PBS-T (PBS/0.2%Tween20 [AppliChem]), and blocked in blocking solution (PBS-T/5%BSA [Sigma]/5% FCS [Biochrom]). Cells were incubated in blocking solution overnight at 4°C containing the following primary antibodies: α-HB9 (homeobox 9), used as MN-specific marker (1:100); AB2145209 from Hybridoma Bank; α-SV2 (Synaptic vesicle glycoprotein 2), used as synaptic vesicle marker; AB2315387 (SV2-c) from Hybridoma Bank; α-CHAT, AB144P from Millipore; α-Tau (axon-specific marker), sc-390476 from Santa Cruz; and α-NCALD. After washing in PBS, cells were incubated with secondary antibodies labeled with AlexaFluor488, AlexaFluor647, or AlexaFluor568 (Invitrogen) in PBS, optionally with phalloidin-AlexaFluor568 (Invitrogen). Cells were washed and mounted on objects slides with Mowiol (Sigma) for imaging.

#### *Endocytosis Assay*

Fibroblasts were plated in DMEM (Invitrogen) and starved for 10 min in starvation media (DMEM transparent [HEPES], 2% FCS) prior to fluorescein isothiocyanate (FITC)-Dextran treatment (5 mg/mL, Sigma) for respective time periods at 37°C. Subsequently, cells were washed with ice-cold PBS and fixed in 4% PFA for 10 min. After washing, cells were stained with phalloidin-AlexaFluor568 and DAPI (Invitrogen) and mounted with Mowiol for imaging.

#### *Flow Cytometry Analysis*

NSC34 cells were transfected with indicated siRNAs for 48 hr prior to 6 hr starvation and incubation with 5 mg/mL FITC-Dextran (Sigma) for 20 min at 37°C. Cells were trypsinized (Trypsin, Sigma) on ice and washed with PBS. Uptake of FITC-Dextran was measured with FACS Calibur (BD Biosciences) and analyzed with Cyflogic software (CyFlo Ltd.). Dead cells were excluded by propidium iodide staining (10 μg/mL, Sigma).

#### *$Ca^{2+}$ Current Recordings in NSC34 and PC12*

Whole-cell recordings were performed at 24°C. Electrodes (tip resistance 2.5–3 MΩ) were made of borosilicate glass (0.86 mm OD, 1.5 mm ID, Science Products) with a temperature-controlled pipette puller (PIP5, HEKA Elektronik) and filled with solution containing (in mM) 133 CsCl, 1 $CaCl_2$, 2 $MgCl_2$, 10 HEPES, and 10 EGTA, adjusted to pH 7.2 and osmolarity of 415 mOsm. During experiments, cells were constantly superfused with saline solution containing (in mM) 84 NaCl, 20 CsCl, 2.5 KCl, 10 $CaCl_2$, 2 $MgCl_2$, 10 HEPES, and 30 glucose, adjusted to pH 7.3 and osmolarity of 310 mOsm. To isolate $Ca^{2+}$ currents, a combination of pharmacological blockers and ion substitution was used. Transient voltage-gated $Na^+$ currents were blocked by tetrodotoxin ($10^{-6}$M TTX, T-550, Alomone). 4-aminopyridine (4AP, $4 \times 10^{-3}$ M, A78403, Sigma) blocked transient $K^+$ currents ($I_A$) and tetraethylammonium (TEA, 2 × 10-3, Sigma) blocked sustained $K^+$ currents ($I_{K(V)}$) and $Ca^{2+}$-activated $K^+$ currents ($I_{K(Ca)}$). The pipette solution did not contain potassium. Whole-cell voltage-clamp recordings were made with EPC10 patch-clamp amplifier (HEKA Elektronik) controlled by Patchmaster program (V2x53, HEKA-Elektronik). Electrophysiological signals were low-pass filtered at 2.9 kHz (3pole Bessel filter). Data were sampled at 50 μs intervals (20 kHz). The offset-potential and capacitance were compensated using "automatic mode" of EPC10 and liquid-junction potential between intracellular and extracellular solution of 2.5 mV (calculated with Patcher's Power-Tools plug-in) was compensated. Whole-cell capacitance was determined using EPC10 capacitance compensation (C-slow). To remove uncompensated leakage and capacitive currents, p/6 protocol was used.[47] Voltage errors due to series resistance (RS) were minimized using RS compensation of EPC10 to 70%–80% with 100 μs time constant (τ).

## Statistical Analysis

#### *Statistical Analysis*

If not mentioned otherwise, all statistical analyses were performed using software programs Excel 2013 (Microsoft), GraphPad Prism 6 (GraphPad Software), and Sigma Plot 11 (Systat Software); ANOVA, Mann-Whitney U test, Fisher's exact test, or unpaired two-tailed Student's t tests were applied. All data are represented as mean ± SEM/SD. Significance of RNA expression and protein levels was tested using a directional Student's t test for uncorrelated samples. For experiments performed in *C. elegans*, Mann-Whitney U test was performed. Significance in the differences of mouse behavioral analyses, NMJ, and muscle fiber surface area size, motor axon length, proprioceptive inputs on MNs, NSC34 neurite length, and width of the synaptic cleft was determined by the use of 1-way ANOVA or directional Student's t test for uncorrelated samples. Survival was analyzed using Kaplan-Meier method by log rank test.

For all studies using mice, animals numbers were calculated prior to experiments by power calculation using the G*Power 3.1.7 software (Power = 0.8 and alpha-error = 0.05). Endpoint criteria for mouse experiments were defined in animal application prior to experiments. Animal samples were processed equally and allocated to experimental groups post-analysis. For all other

experiments, sample size was estimated based on the known variability of the assay.

Values of $p < 0.05$ were considered significant. In all cases, three levels of statistical significance were distinguished: *$p < 0.05$, **$p < 0.01$, and ***$p < 0.001$.

Specific statistical tests, sample size, and p values are indicated in the figure legends.

#### *Statistical Analysis of Electrophysiology*

Data were analyzed using Spike2 and statistical analysis was performed in GraphPad Prism 5.05 (GraphPad Software). All calculated values are shown as mean ± SEM. The EEP frequencies for each cell were measured as mean frequencies over 30 s intervals. Frequencies before and during NMDA application were compared by a paired t test for each group. Kruskal-Wallis test followed by Dunns multiple comparisons was used to compare EPP frequencies in different groups. A significance level of $p < 0.05$ was accepted for all tests.

## Results

### Identification of NCALD as a Potential SMA Modifier by Genome-Wide Linkage and Transcriptome-Wide Differential Expression Analysis

In a four-generation Mormon family from Utah, we identified seven individuals carrying homozygous *SMN1* deletions, two affected by type 1 SMA and five fully asymptomatic, except for increased photosensitivity (Figure 1A; see Supplemental Data for full clinical investigation description of Utah family members).

Haplotype analysis of SMA regions showed a co-segregation of three different SMA alleles (Figure 1A). The two type 1 SMA-affected individuals carried no *SMN1* and two *SMN2* copies. By contrast, all five asymptomatic individuals showed homozygous absence of *SMN1* and presence of four *SMN2* copies, resembling a genotype associated with type 3 SMA[13] (Figure 1A). *SMN2* sequencing excluded any further variants affecting expression. In lymphoblastoid cells (LBs), SMN RNA and protein levels were similar to those in typical type 3 SMA-affected individuals, thus excluding *cis*- and *trans*-acting factors regulating *SMN2*. Increased *PLS3* expression was not found (Figure 1A; GEO: GSE58316). Thus, we concluded that a previously unknown SMA modifier potentially protects these individuals.

To identify the SMA modifier, we combined linkage with transcriptome-wide differential expression analysis. Assuming a dominant mode of inheritance, a parametric linkage analysis with 14 family members revealed 8 positive peaks with a maximum LOD score of 1.5 (Figure 1B). In parallel, a transcriptome-wide differential expression analysis with 12 total RNA samples was performed (GEO: GSE58316) and revealed 17 transcripts significantly differentially regulated in asymptomatic individuals (Table S2). *NCALD* was represented by two independent hybridization probes on the array, both showing a 4- to 5-fold downregulation in the asymptomatic group versus familial type 1 SMA or an independent type 3 SMA group. Most importantly, *NCALD* was the only transcript localized in one of the eight linked regions on chromosome 8q22.3 (between rs28144 and rs958381), making it a highly likely candidate. Microarray data were confirmed by qRT-PCR and western blot (Figures 1C and 1D).

To search for the potential genetic mechanisms involved in reduced *NCALD* expression, targeted resequencing of ~3 Mb genomic DNA encompassing *NCALD* in five family members was carried out. On average 2,723 variants were called per sample. Based on previous haplotype data, we filtered for heterozygous variants shared between individuals II-1, III-1, III-4, and IV-3 but absent in III-8. This yielded 43 variants (21 previously annotated SNPs), none of which were in the *NCALD* coding region. Only the SNP rs147264092 in intron 1 (HGVS: NC_000008.10: g.103128181_103128182insCT) with a minor allele frequency (MAF) = 0.11 (1000 Genomes) was located in *NCALD* UTR (Table S3). Approximately 600 kb upstream of *NCALD*, we identified a 17-bp deletion (HGVS: NC_000008.10: g.103783522_103783538del17; dbSNP: rs150254064; 1000 Genomes: MAF = 0.04) perfectly segregating with the modifier haplotype (Figure S1) that seemed interesting. The 17-bp deletion is localized adjacent to an H3K27AC block and a super enhancer (ENCODE), which may influence *NCALD* expression. We hypothesize that the combination of both variants acts on *NCALD* expression (unpublished data). Both variants were further analyzed in 50 *SMN1*-deleted individuals, who were chosen because of a discrepant SMA severity according to their *SMN2* copy number, and 65 controls. The combination of both variants was found in one individual, who unexpectedly carried only one *SMN2* copy. This genotype is regarded as a type 0 SMA with death in utero or immediately after birth.[48] In contrast, this individual survived 9 months, suggesting a potential protection by a genetic modifier, which could be *NCALD*. No LBs were available to test expression. The combination of both variants on a haplotype is a very rare event: 0.003 (13/5,008 haplotypes included in the Phase 3 1000 Genomes project, see LDlink). Since homozygous deletions of *SMN1* occur with a frequency of 1:6,000 to 1:20,000 depending on ethnicity,[49] the combination of homozygous *SMN1* deletion and the chromosome 8 modifier haplotype would statistically occur in fewer than 1:8,000,000 people. Further work is in progress to fully understand the impact of these variants on chromatin structure and *NCALD* expression. However, since understanding gene regulation and the interplay between *cis*- and *trans*-regulatory elements is extremely challenging and may not yield solid results, we decided to take the direct approach and analyze the impact of NCALD reduction in four different SMA animal models: *C. elegans*, zebrafish, and a severe and a mild SMA mouse model.

NCALD is one of 14 neuronal calcium sensor (NCS) proteins in mammals. These proteins are highly conserved across species and primarily involved in neuronal $Ca^{2+}$ signaling.[50,51] *NCALD* encodes a ~22 kDa protein that contains two pairs of EF-hand domains and an N-terminal

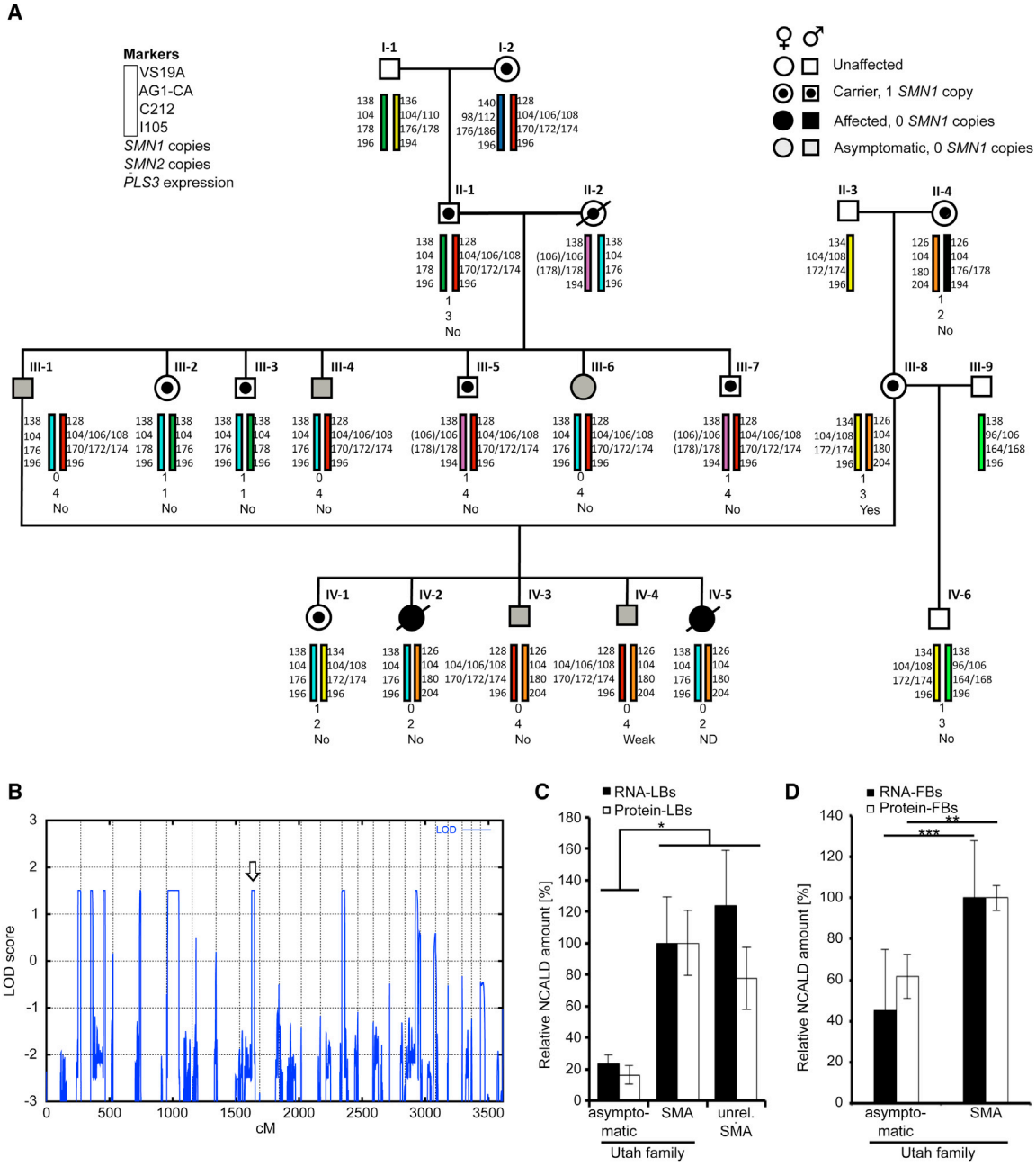


**Figure 1. Genome-wide Linkage and Transcriptome Analysis Uncovered NCALD as Candidate Modifier of SMA**

(A) Pedigree of the Utah family: haplotype analysis of microsatellite markers in the 5q13 SMA region and *SMN1* and *SMN2* copies are indicated. Black filled symbols indicate SMA-affected individuals; gray filled symbols indicate asymptomatic *SMN1*-deleted individuals; and symbols with a dot indicate SMA carriers. Quantification of *PLS3* expression in LBs was done according to Oprea et al.[24] Note that weak *PLS3* have no impact on SMA phenotype.[24]

(B) Genome-wide linkage analysis identified eight regions with positive LOD scores. Open arrow marks 8q22.3 region containing *NCALD*.

(C) Verification of microarray results (Table S2) of *NCALD* RNA and protein in lymphoblastoid (LB) cells (NCALD levels are relative to NCALD in SMA-affected individuals of the Utah family [set to 100%]). *NCALD* is represented by two independent probes on the expression array, showing a 4- to 5-fold downregulation in the asymptomatic group versus familial type 1 SMA or an independent type 3 SMA group. Three independent experiments including all 17 cell lines (asymptomatic, n = 5; symptomatic, n = 2; independent SMA-III, n = 10) were performed. Error bars indicate SD; *$p \leq 0.05$.

(D) Expression analysis of *NCALD* RNA and proteins in fibroblasts (FB) derived from the Utah family (asymptomatic, n = 5; symptomatic, n = 2). Three independent experiments including all seven cell lines were performed. Error bars indicate SD; **$p \leq 0.01$; ***$p \leq 0.001$.

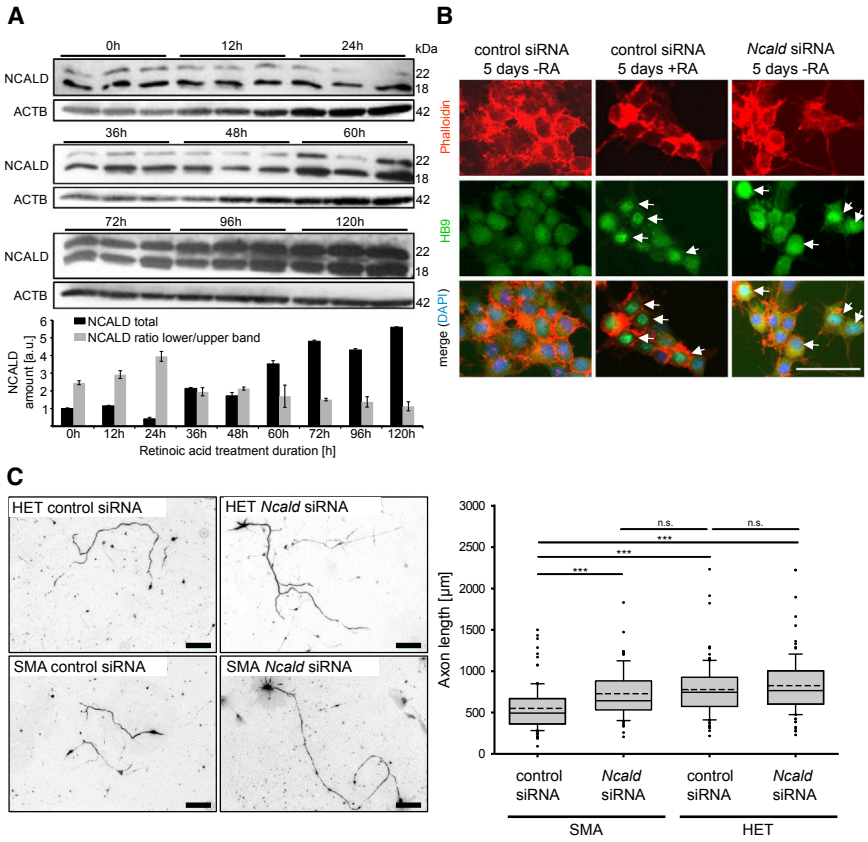


**Figure 2. NCALD Downregulation Restores Neurite Outgrowth Defect in SMN-Deficient Neuronal Cells**

(A) Western blot of NSC34 cells treated with 1 μM retinoic acid (RA) for 0–120 hr as a model of MN differentiation and maturation (n = 3 independent experiments). Error bars indicate SEM.

(B) *Ncald* siRNA-treated NSC34 cells show signs of MN differentiation (HB9-positive staining, marked with white arrows) even in absence of RA (right). As positive control, cells were differentiated with RA and treated with control siRNA (middle). Negative control was treated only with control siRNA (left). Scale bar represents 100 μm.

(C) Primary MNs from SMA or HET murine embryos were fixed at 8 DIV and stained with anti-neurofilament M (anti NF-M). Quantitative analysis of axon length of MNs. SMA: n = 7, HET: n = 6, n = 100 per measurement; ***p ≤ 0.001; dashed line indicates mean; straight line indicates median; values covered from 25%–75% and dotted outliers at <5% and >95% CI. Scale bars represent 100 μm.

myristoyl anchor, which enables switching from cytosolic to membrane-bound forms in a $Ca^{2+}$-dependent manner.[52,53] A $Ca^{2+}$-dependent mobility shift of both myristoylated and non-myristoylated forms was reported.[54] NCALD is highly abundant in cerebral neurons, spinal MNs, and in axonal growth cones.[55] NCALD overexpression inhibits neurite outgrowth.[56] NCALD is important in phototransduction,[57] which may explain photosensitivity in asymptomatic individuals. Importantly, NCALD interacts with clathrin and actin, both of which are involved in endocytosis and synaptic vesicle recycling.[58,59]

## NCALD Knockdown Triggers MN Differentiation and Restores Neurite and Axonal Growth in SMA

First, we analyzed NCALD levels during MN differentiation and maturation in NSC34 cells treated with retinoic acid (RA)[60] to induce differentiation and observed a steady increase in NCALD amount over time under RA treatment (Figure 2A). siRNA-mediated *Ncald* reduction (Figure S2A) induced MN differentiation (indicated by HB9-positive staining) and triggered neurite outgrowth even without RA treatment (Figure 2B). In contrast, NCALD overexpression in RA-treated NSC34 cells impaired neurite outgrowth (Figures S2B and S2C). NCALD is highly abundant in axonal growth cones of spinal MNs.[55] In addition, we show that it localizes at the presynaptic terminals of NMJs, suggesting a potential role at the NMJ (Figures S2D and S2E).

We found that *Ncald* knockdown in *Smn*-deficient NSC34 cells restored impaired neurite outgrowth to control levels (Figure S2E). Similar results were obtained in cultured primary MNs from SMA ($Smn^{ko/ko}$; $SMN2^{tg/0}$) versus HET ($Smn^{ko/wt}$;$SMN2^{tg/0}$) embryos, where reduced axon length of SMA MNs[61] was restored by siRNA-mediated *Ncald* knockdown (Figure 2C). These findings indicate that reduced NCALD levels counteract the impaired axonal development of SMN-deficient MNs.

## *ncald* Knockdown Restores Axonal Growth and NMJ Functionality in Zebrafish *smn* Morphants

Human NCALD and its ortholog in zebrafish are 98% identical, suggesting important conserved functions across species. We next investigated the modifying effect of *ncald* in vivo in a *mnx1:eGFP*-expressing zebrafish line[40] by MO-mediated knockdown of either *smn*, *ncald*, or both together. Consistent with previous results, *smn* depletion resulted in motor axon-specific outgrowth defects, such as truncations and ectopic branches[24,62] (Figure 3A). Knockdown of *ncald* led to enhanced motor axons branching, whereas double *smn*+*ncald* knockdown fully rescued the truncated motor axon defect associated with Smn deficiency (Figures 3A, 3C, and S3A). Knockdown efficiency was confirmed by western blot (Figure 3B). We also found that overexpression of human *NCALD* mRNA in wild-type zebrafish caused truncation and branching of motor axons (Figure S3B), resembling the phenotype of *smn* morphant zebrafish (Figure 3A) similar to NSC34 cells (Figure S2C).

During NMJ maturation, the width of the synaptic cleft is increasing, which is essential in neurotransmission.[63] Ultrastructural analysis of the synaptic cleft revealed an

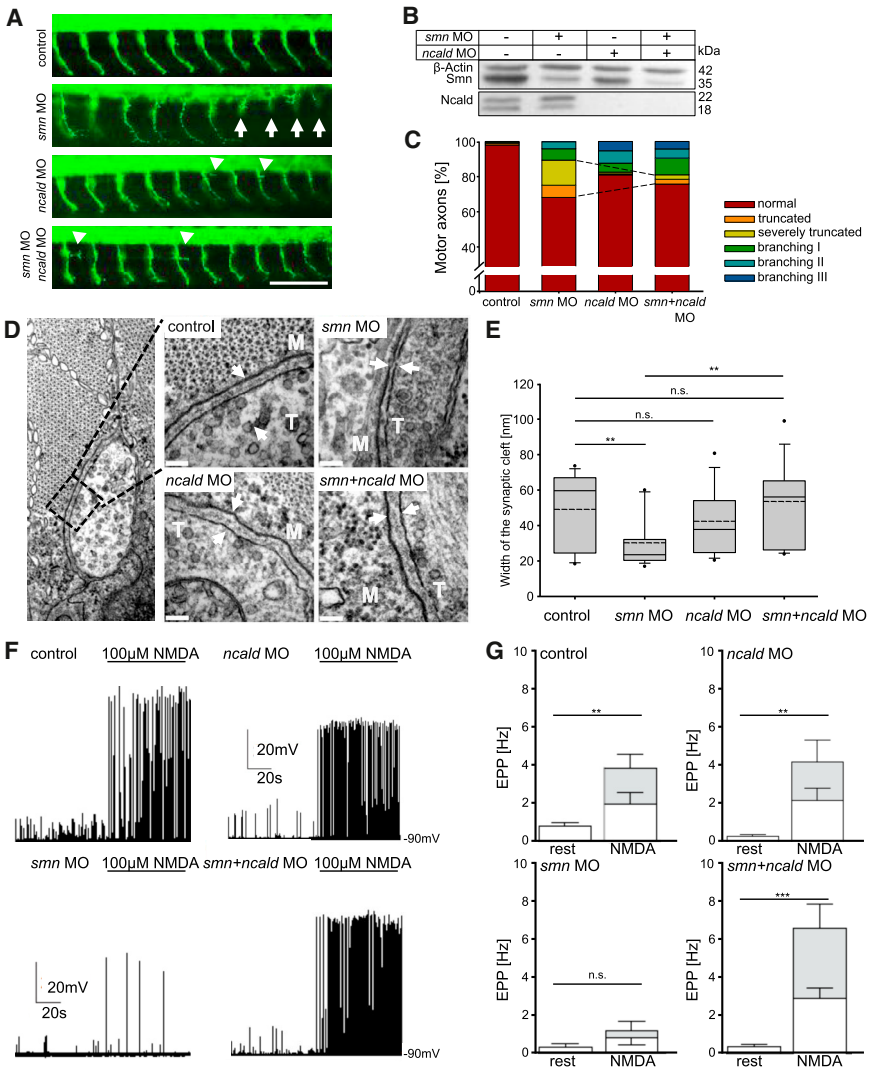


**Figure 3. *Ncald* Reduction Corrects the Phenotype in *Smn*-Deficient Zebrafish**

(A) First 10 motor axons posterior to the yolk globule of 34 hpf zebrafish embryos injected with respective morpholinos (MO). White arrows mark truncated motor axons. Arrowheads mark extensive branching in *ncald* or *smn*+*ncald* morphants; green shows Znp1 staining, for motor axons. Scale bar represents 100 µm.

(B) Western blot of lysates of zebrafish embryos injected with indicated MO.

(C) Quantification of motor axon phenotype. Dashed lines mark the rescue of the truncation phenotype (**p ≤ 0.01). *smn*+*ncald* and *ncald* morphants showed increased branching. n > 500 motor axons per MO injection.

(D) TEM images of NMJs of 48 hpf zebrafish embryos injected with respective MO. White arrows mark synaptic clefts including basal lamina. M indicates muscle fiber, T indicates nerve terminal. Scale bars represent 100 nm.

(E) Quantification of synaptic cleft width of MO-injected 48 hpf fish (n = 15 per treatment). **p ≤ 0.01, dashed line indicates mean; straight line indicates median; values covered 24%–75% and dotted outliers at <5% and >95% CI.

(F and G) Whole-cell current clamp recordings EPPs (F) and quantification (G) of mean EPP frequencies in ventral fast muscle cells of control (n = 12), *smn* (n = 10), *ncald* (n = 11), and *smn*+*ncald* (n = 12) morphants under control conditions or NMDA induction. White bar parts reflect the mEPP frequencies, gray bar parts reflect the frequency of the TTX-sensitive large EPPs. **p ≤ 0.01; ***p ≤ 0.001. Error bars indicate SEM.

impaired NMJ maturation in *smn* morphants (Figures 3D and 3E). The width of the synaptic cleft in *smn* morphants was significantly smaller than in controls or *ncald* morphants; double *smn*+*ncald* knockdown significantly restored synaptic maturation, resulting in a cleft width similar to control embryos (Figures 3D and 3E).

To test the functionality of neuromuscular synapses between caudal primary MNs and ventral fast muscle cells,[64] we performed whole-cell patch clamp recordings from muscle cells during MN stimulation in control (ctrl), *smn*, *ncald*, and *smn*+*ncald* zebrafish morphants. We recorded spontaneous endplate potentials at rest (without stimulation) and during MN stimulation by NMDA (N-methyl-D-aspartate, agonist of NMDA receptors) (Figure S3C). In controls, we recorded at rest small endplate potentials that were primarily not tetrodotoxin (TTX) sensitive (Figures S3D and S3E) and mostly resembled miniature endplate potentials (mEPPs).[65] During NMDA stimulation, the mEPP frequency did not significantly increase, but large TTX-sensitive endplate potentials and muscle action potentials were induced by MN spike-evoked transmission. In *smn* morphants, a significantly lower spontaneous mEPP frequency and only occasional action potentials during NMDA stimulation were observed (Figure 3F). In the *smn*+*ncald* morphants, the spontaneous mEPP frequency was slightly increased and the frequency of large NMDA-induced EPPs was restored to control levels (Figures 3F and 3G). In line with the electrophysiological data, swimming velocity after electrical stimulation was reduced in *smn* morphants but rescued in *smn*+*ncald* morphants (Figure S3F). Together, these results show that Ncald knockdown rescues neural circuit function at the NMJs of *smn* morphants.

## Loss of NCALD Ortholog Suppresses Defects of *C. elegans* SMA Model

*C. elegans* lacking the *SMN* ortholog *smn-1*, referred to here as *Cesmn-1*, show neuromuscular defects, including decreased pharyngeal pumping rate (Figure S4A).[26,41] The *C. elegans* ortholog of *NCALD* is encoded by neuronal calcium sensor-1 (*ncs-1*).[66] Either *ncs-1* knockdown by RNA interference or introduction of the *ncs-1(qa401)*

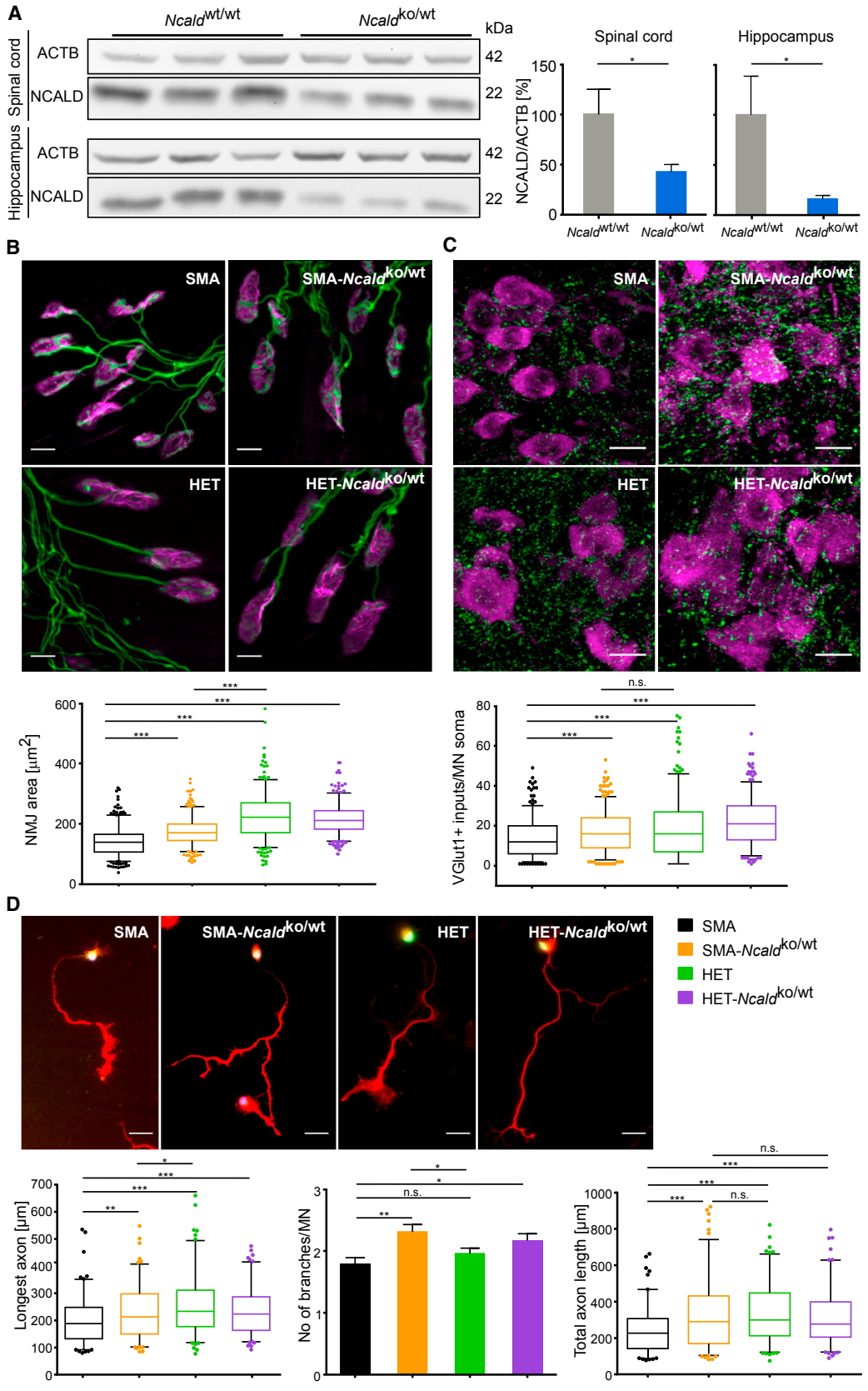


**Figure 4. Heterozygous *Ncald* KO Improves Axonal Outgrowth, Proprioceptive Input, and NMJ Size in Severe SMA Mice**
(A) Western blot and quantification of NCALD and ACTB (loading control) in spinal cord and hippocampus of P10 WT and *Ncald*$^{ko/wt}$ mice. *p $\leq$ 0.05. Error bars indicate SD.

*(legend continued on next page)*

loss-of-function allele in *Cesmn-1* animals significantly ameliorated pumping defects (Figures S4B and S4C), confirming that NCALD loss ameliorates the SMN loss-of-function-induced neuromuscular defects across species.

### Heterozygous *Ncald* KO Ameliorates Motor Neuron Development in Severe SMA Mice

We took advantage of an *Ncald* knockout mouse ($Ncald^{ko/ko}$) recently generated by the Knockout Mouse Phenotyping Program at the Jackson Laboratory. Heterozygous $Ncald^{ko/wt}$ mice are asymptomatic and show >50% reduction of NCALD levels in spinal cord and brain (Figure 4A). Homozygous $Ncald^{ko/ko}$ mice are viable and fertile; however, preliminary reported data by the International Mouse Phenotype Consortium (IPMC) (online database) and our data revealed behavioral abnormalities, vision defects, and metabolic impairment. In contrast, heterozygous $Ncald^{ko/wt}$ mice showed no gross morphological or behavioral problems even at 18 months of age. Since asymptomatic individuals show reduced but not full loss of NCALD, we used the heterozygous $Ncald^{ko/wt}$ animals for all further experiments herein.

The $Ncald^{ko/wt}$ allele was bred into a severe SMA mouse model[9] on pure C57BL/6N background. Both SMA and SMA-$Ncald^{ko/wt}$ mice die at a mean age of 13 days and there is no difference in weight progression at this age (Figures S5A and S5B). Severe SMA mice show multi-organ failure[27,43,67] due to very low SMN levels, which could not be rescued by heterozygous *Ncald* knockout alone. Nonetheless, we found that other hallmarks of SMA were improved upon heterozygous *Ncald* knockout: the size of the NMJs in the transversus abdominis muscle (TVA) was increased and the number of proprioceptive inputs on MN soma was elevated in SMA-$Ncald^{ko/wt}$ versus SMA mice (P10) (Figures 4B and 4C). Moreover, SMA-$Ncald^{ko/wt}$ mice showed more inputs per MN than SMA mice independent of cell size (Figure S5C). A comparison of axonal development in cultured primary MNs revealed a large impact of NCALD reduction on axonal growth and arborization (Figure 4D), confirming our initial results with siRNA-mediated *Ncald* knockdown (Figure 2C). Therefore, NCALD reduction counteracts impaired axonal development and restores NMJ size in SMN-deficient mice but is not able to improve survival due to severe multiple organ impairment.

### Combinatorial Therapy with a Suboptimal Low-Dose SMN-ASO and Reduced *Ncald* Expression Ameliorates SMA Pathogenesis in a Severe SMA Mouse Model

In our study, we combined suboptimal low-dose SMN-ASOs with heterozygous *Ncald* knockout mice for four reasons: (1) asymptomatic individuals carry four *SMN2* copies, similar to typical type 3 SMA-affected individuals, but not two *SMN2* copies as our severe SMA mouse model or most type 1 SMA-affected individuals; (2) genetic modifiers efficiently protect against SMA only if a sufficient SMN level is present to suppress inner organ dysfunction;[29] (3) NCALD expression is mainly restricted to neuronal tissues, so its beneficial effect is directed to MN, but cannot improve other peripheral organs affected in severe type of SMA; and (4) type 1 SMA-affected individuals, currently treated with SMN-ASOs, show only a moderate SMN elevation and may need additional drugs/molecules supporting MN function. For these reasons, we chose to establish a mild SMA mouse model that shows no impairment in lifespan or peripheral organs, but has a prominent motoneuronal phenotype. Since presymptomatic subcutaneous (s.c.) injection of high-dose SMN-ASO in severely affected SMA mice fully rescues SMA[68] and low-dose SMN-ASO in C57BL6/N congenic mice increased survival to only 1 month (intermediate phenotype),[29] we opted for a different strategy to produce a mild SMA phenotype. We crossed C57BL/6N $Ncald^{ko/wt}$;$Smn^{ko/wt}$ males with FVB/N $Smn^{ko/ko}$;$SMN^{tg/tg}$ females to produce 50% C57BL/6N:50% FVB/N ($mixed_{50}$) offspring (Figure 5A). This breeding strategy was already performed previously and showed increased lifespan and more robustness when compared to pure C57BL6/N or FVB/N mice.[27] However, almost as expected, untreated $mixed_{50}$ SMA and SMA-$Ncald^{ko/wt}$ mice live 16.5 and 17.0 days, respectively, showing that the modifier alone is still unable to counteract the massive loss of SMN (Figure 5B). Therefore, $mixed_{50}$ offspring were injected s.c. with a single suboptimal dose (30 μg) of SMN-ASO on P1. Elevated SMN levels were obtained in liver, but not in spinal cord or brain (Figure S6A). Survival of SMA+ASO mice was rescued (Figure 5B), but their motoric abilities were visibly impaired as determined by righting reflex and grip strength tests (Figures 5C and 5D). This suggests that slightly elevated SMN levels achieved by systemic SMN-ASO treatment rescued non-neuronal multi-organ impairment,[29] but not MN function. In contrast, heterozygous

(B) Representative images and quantification of NMJ area ($\mu m^2$) in TVA muscle from P10 mice stained with antibodies against NF-M and SV2 (green, for presynaptic terminals) and Bungarotoxin (magenta, for postsynapse). NMJ area was analyzed with ImageJ software (N = 3, n = 100–120 NMJs/mouse). ***$p \leq 0.001$. Scale bars represent 10 μm.
(C) Representative images and quantification of proprioceptive inputs (VGLUT1, green) on MN soma (CHAT, magenta) in lumbar spinal cord sections from P10 mice. Mean input number within 5 μm of MN soma was analyzed (N = 3, n = 100–120 MNs/mouse). ***$p \leq 0.001$. Scale bars represent 25 μm. Note, color code for genotypes is identical to (D).
(D) Representative merged images of 6 DIV MNs isolated from E13.5 embryos and stained with DAPI (blue, for DNA) and antibodies against HB9 (green, for MN) and Tau (red, for axon). The longest axon and axonal branches were quantified with ImageJ (N = 3–5, n = 20–40 axons per mouse). Scale bars represent 25 μm. Each boxplot covers values from 25%–75% with line at median and dotted outliers at <5% and >95% CI. For each experiment, image analysis was double-blinded. n.s. indicates non-significant; *$p \leq 0.05$; **$p \leq 0.01$; ***$p \leq 0.001$.

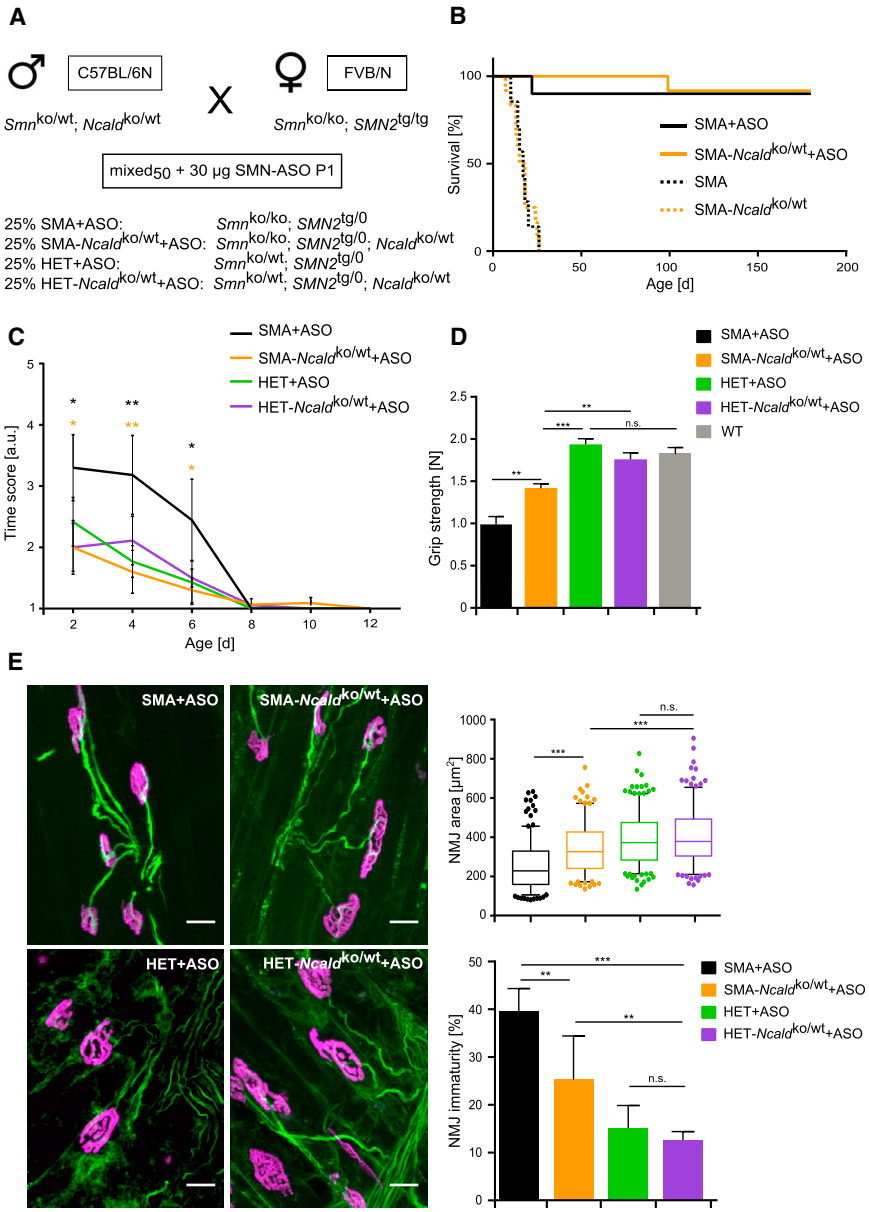


**Figure 5. NCALD Reduction Improves Motoric Function, NMJ Size, and NMJ Architecture in SMA+ASO Mice**

(A) Breeding scheme to produce mixed$_{50}$ SMA and HET mice. All mixed$_{50}$ offspring were injected with 30 µg SMN-ASO at P1.

(B) Kaplan-Meier curves of uninjected mixed$_{50}$ mice show no differences in survival between SMA (17 days, N = 7) and SMA-*Ncald*$^{ko/wt}$ (16.5 days, N = 12). Injection of 30 µg SMN-ASO on P1 increases survival to >180 days for both SMA+ASO (N = 10) and SMA-*Ncald*$^{ko/wt}$+ASO (N = 12) mice.

(C) Righting reflex test shows improvement in SMA-*Ncald*$^{ko/wt}$+ASO but not SMA+ASO mice during P2–P6 (n ≥ 12 per genotype). Error bars represent SEM; n.s. indicates non-significant, **p ≤ 0.01, ***p ≤ 0.001.

(D) Grip strength test performance at P73 reveals enhanced strength for SMA-*Ncald*$^{ko/wt}$+ASO mice compared to SMA-+ASO mice (N ≥ 12 per genotype). Error bars indicate SEM. *p ≤ 0.05, **p ≤ 0.01, ***p ≤ 0.001.

(E) Representative images of NMJs of ASO-treated mixed$_{50}$ mice at P21 stained with the antibody against NF-M (green, for presynaptic terminal) and Bungarotoxin (magenta, for postsynaptic terminal). Scale bars represent 20 µm. Boxplot shows quantification of NMJ area in µm$^2$ in TVA muscle which was analyzed and represented as in Figure 4. Bar graph shows percentage of immature NMJs in TVA muscle (mean ± SD). N = 3 mice per genotype; n = 60–100 NMJs per mouse. n.s. indicates non-significant, *p ≤ 0.05, **p ≤ 0.01, ***p ≤ 0.001.

*Ncald* knockout, in addition to low-dose SMN-ASO treatment, significantly improved motoric abilities (Figures 5C and 5D). Analysis of NMJ maturation score on P21[45] showed that both NMJ size and maturation were markedly restored by *Ncald* reduction as compared to SMA+ASO mice (Figure 5E). Heterozygous *Ncald* knockout did not rescue tail necrosis and slightly impacted weight progression in male mice (Figures S6B–S6D). Our data provide conclusive evidence of the beneficial effect of reduced NCALD on the neuromuscular system and motoric function in SMA+ASO mice.

## Low SMN Decreases $Ca^{2+}$ Influx in NSC34 and PC12 Cells

Since NCALD is a neuronal $Ca^{2+}$ sensor and impaired $Ca^{2+}$ homeostasis has been reported in SMA,[69] we tested whether lowering SMN and NCALD levels could modulate voltage-dependent $Ca^{2+}$ currents ($I_{Ca}$) in MN-like cells. We performed whole-cell patch-clamp recordings and ratiometric $Ca^{2+}$ imaging with fura-2. We recorded $I_{Ca}$ of RA-differentiated NSC34 cells that were treated with siRNAs specific to *Smn*, *Ncald*, or *Smn*+*Ncald* and analyzed the $I_{Ca}$ tail currents with a series of increasing voltage pulses. In NSC34 cells, *Smn* depletion significantly reduced the voltage-dependent $Ca^{2+}$ influx, which was not restored by additional NCALD reduction (Figure 6A). Ratiometric $Ca^{2+}$ imaging with fura-2 revealed a reduced voltage-dependent $Ca^{2+}$ influx in SMN-depleted PC12 cells compared to controls (Figure S7A). These data show that low SMN levels impair $Ca^{2+}$ influx, which is not restored by NCALD knockdown and that NCALD depletion rescues synaptic transmission through a different mechanism.

## Disturbed Endocytosis and Synaptic Vesicle Recycling Is Ameliorated by NCALD Depletion

We next sought for a common pathway in which both SMA modifiers, NCALD and PLS3, might operate. Since

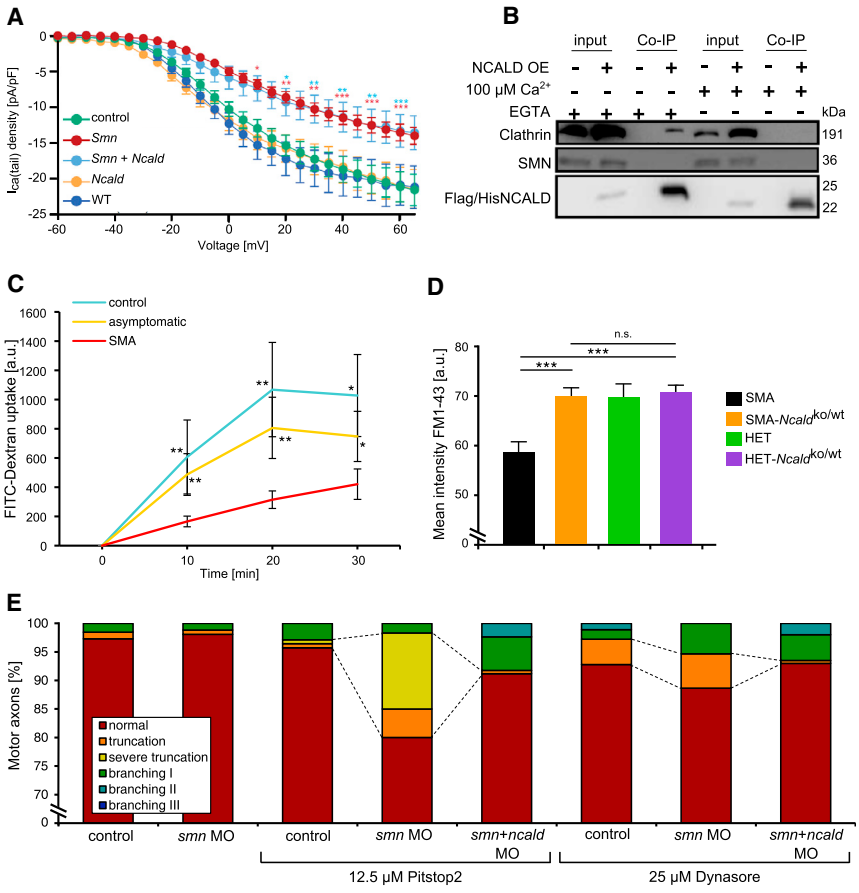


**Figure 6. Interconnection between SMN, NCALD, Voltage-Dependent $Ca^{2+}$ Influx, Endocytosis, and SMA**

(A) Measurement of *I-V* relations of $Ca^{2+}$ tail currents in differentiated NSC34 cells treated with respective siRNAs and depolarized for 5 ms to 60 mV, in 5 mV increments, at holding potential −80 mV. Currents were not different between wild-type (n = 7), control siRNA (n = 33), and *Ncald* KD (n = 13) and were significantly reduced upon *Smn* KD (n = 15) and *Smn+Ncald* KD (n = 12) at current pulses above −35 mV. *p ≤ 0.05; **p ≤ 0.01; ***p ≤ 0.001. Error bars indicate SEM.

(B) Western blot of co-immunoprecipitation experiment. NSC34 cells were transiently transfected with FLAG-His-NCALD or control vector. Co-immunoprecipitations with FLAG-M2 affinity beads were performed in the presence or absence of $Ca^{2+}$. NCALD interacts with clathrin only in the absence of $Ca^{2+}$ (addition of EGTA to the cell lysate) but not in the presence. Note the positive clathrin band in the test-Co-IP (fourth lane) in the absence but not in the presence of $Ca^{2+}$ (last lane).

(C) Quantification of endocytosis by FITC-dextran uptake in fibroblasts from SMA (n = 10), controls (n = 3), and asymptomatic individuals (n = 5); n = 50 per cell line and time point. Mean ± SD. *p ≤ 0.05, **p ≤ 0.01.

(D) Quantification of FM1-43 intensity at presynaptic terminals in TVA muscles under low-frequency stimulation (5 Hz, 1 s). n = 3 per genotype, n ≈100 per mouse. Mean ± SEM; n.s. indicates non-significant; ***p ≤ 0.001.

(E) Quantification of MN axon phenotype of zebrafish embryos treated with sub-phenotypical doses of *smn* MO (2 ng), *ncald* MO (2 ng), and the endocytosis inhibitors Pitstop2 and Dynasore, respectively. Dashed lines highlight the synergistic effect of *smn* MO and Pitstop2 and the effect of Dynasore on axon truncation. Additional *ncald* MO injection ameliorates the truncation defect. ***p ≤ 0.001. Motor axons per treatment: Pitstop2: n ≥ 100, Dynasore: n ≥ 150.

NCALD binds clathrin directly[58] and PLS3 knockout in yeast impairs endocytosis,[58,70] we hypothesized that low SMN levels may impair endocytosis, which in turn is rescued by reduced NCALD or increased PLS3 levels. Indeed, we recently reported impaired endocytosis as a disturbed cellular mechanism affected in SMA, which is rescued by elevated PLS3 levels.[29] Impaired endocytosis and endocytic trafficking have further been demonstrated in a *C. elegans* SMA model.[71]

Co-immunoprecipitation studies in NSC34 cells revealed NCALD interaction with clathrin only in the absence of $Ca^{2+}$ (Figure 6B) or at low $Ca^{2+}$ levels (data not shown). TEM analyses after immunogold staining of wild-type zebrafish sections showed co-localization of Ncald and clathrin in the presynaptic sites of NMJs (Figure S7B).

To study the effect of NCALD on endocytosis, we undertook FITC-dextran internalization assays in various cell culture systems. In primary fibroblast cell lines derived from SMA-affected individuals, endocytosis rates were strongly reduced compared to controls but were restored in fibroblasts of asymptomatic individuals (Figures 6C and S7C). Moreover, *Smn* knockdown in NSC34 cells significantly reduced FITC-dextran uptake, which was rescued by concomitant *Ncald* knockdown. *Ncald* knockdown alone increased the rate of endocytosis by 1.3-fold, demonstrating that low NCALD levels already facilitate endocytosis (Figure S7F).

Moreover, we analyzed endocytic uptake of FM1-43 in mouse NMJs under stimulation at 5 and 20 Hz as described.[29] FM1-43 uptake was markedly decreased in SMA mice at 5 Hz stimulation (triggering clathrin-dependent endocytosis), but heterozygous *Ncald* knockout fully restored the levels similar to HET mice (Figures 6D and S7D). Heterozygous *Ncald* knockout had no impact at 20 Hz stimulation (triggering bulk endocytosis), further strengthening the specific role of NCALD in the clathrin-dependent endocytosis at the NMJ (Figure S7E).

Lastly, we investigated in vivo the mutual effect of endocytosis and the Smn-Ncald-clathrin network for SMA using pharmacological inhibition of endocytosis in zebrafish. Using sub-phenotypical concentrations of either *smn* MO (2 ng) or a suboptimal dose of Pitstop2 (12.5 µM), an

inhibitor of clathrin,[72] showed almost no axon truncation and branching phenotype as compared to higher concentrations of *smn* MO (4 ng, Figures 3A and 3C) or Pitstop2 (25 μM, Figure S7G). Instead, combination of suboptimal *smn* MO (2 ng) together with suboptimal Pitstop2 (12.5 μM) resulted in severe motor axons truncation, suggesting a synergistic effect. Notably, this SMA phenotype was strongly ameliorated by additional *Ncald* reduction (Figures 6E, 3A, and 3C). Moreover, the treatment with Dynasore (25 μM), an inhibitor of the endocytosis-driving GTPase dynamin,[73] either alone or in combination with low *smn* MO, resulted in an SMA-like axonal truncation (Figure 6E). These defects were ameliorated by additional treatment with *ncald* MO (Figures 6E and S7G). Together, these findings suggest that SMN and clathrin interact genetically to promote endocytosis and MN axonogenesis, whereas NCALD negatively interferes with an SMN-dependent function of clathrin.

## Discussion

Here, we describe NCALD as a genetic SMA modifier in humans. In summary, we show the following. (1) Reduced NCALD levels protect individuals from developing SMA, despite lacking *SMN1* and carrying only four *SMN2* copies, usually causing type 3 SMA.[13] Thus, unlike PLS3, which alleviates SMA pathology upon overexpression,[24] NCALD reduction acts as a genetic suppressor of SMA. (2) NCALD is localized at SMA relevant sites including MN soma and growth cones as well as the presynaptic site of the NMJ. Furthermore, NCALD knockdown is relevant for MN differentiation and restores neurite and axon outgrowth in MNs or MN-like cells. (3) NCALD has a $Ca^{2+}$-dependent interaction with clathrin and is thereby able to modulate endocytosis and likely vesicle recycling at the motor endplate. (4) NCALD knockdown rescues neural circuit function of zebrafish *smn* morphants by restoring axonal outgrowth defects, endplate potentials, and swimming velocity. (5) *ncs-1* knockdown in *smn-1*-deficient *C. elegans* restores pumping to normal rates. (6) Heterozygous *Ncald* knockout in severely or intermediately affected SMA mice causes clear improvements on the structural level, such as NMJ size and architecture, MN outgrowth, and proprioceptive inputs. (7) Heterozygous *Ncald* knockout in mild SMA mice with no lifespan impairment has beneficial effects on NMJ size and architecture as well as motoric abilities. (8) Finally, across species, the mechanism by which reduced NCALD level improves SMA pathology is restoration of endocytic function, strengthening the existing models holding endocytosis as a main impaired cellular mechanism in SMA.

### NCALD Downregulation as a Potential Therapy in Combinatorial Approach

Clinical trials using ASOs to correct *SMN2* splicing are highly promising and close to FDA approval.[2] However, for type 1 SMA-affected children with only two *SMN2* copies, these approaches are likely insufficient to fully suppress SMA symptoms. It is also unclear to what extent the elevation of SMN after disease onset will be able to protect from SMA and whether combinatorial therapies including SMN-dependent and SMN-independent pathways will be required to achieve full and long-term rescue.[74] There is increasing evidence—at least in mouse models—that systemic SMN elevation is required to fully counteract SMA; systemic injection of SMN-ASOs or AAV9-SMN led to a robust survival increase in various SMA mouse models in comparison to a central nervous system (CNS)-restricted application.[68,75] This is in line with the observation that additional non-neuronal organs and tissues are impaired in severe SMA mouse models and partially in type 1 SMA-affected individuals (reviewed in Hamilton and Gillingwater[18] and Shababi et al.[76]).

Recently, we have shown that PLS3 overexpression in combination with low SMN elevation using SMN-ASOs[68] increased the survival of severely affected SMA mice from 14 to >250 days.[29] This might resemble a hypothetic situation in which individuals with type 1 SMA are treated with a molecule or drug that increases SMN levels acting on the endogenous *SMN2* copies in combination with an additional molecule or drug acting on the genetic modifier. In contrast to PLS3, the effect of NCALD was less pronounced, which is in line with the observation that asymptomatic individuals protected by reduced NCALD require the presence of four *SMN2* copies, while in case of elevated PLS3, three *SMN2* copies are sufficient.[24,25] In addition, the limited effect of NCALD might be due to the restricted expression in neuronal tissues as compared to PLS3, which is ubiquitously present. Moreover, the broader impact of PLS3 on F-actin dynamics that influences various cellular processes at NMJ level[27,29] may further contribute to the more prominent protection.

Nonetheless, a combinatorial therapy that both elevates SMN and decreases NCALD (e.g., by ASO treatment) may provide a full protection, resulting in asymptomatic individuals. The advantage of NCALD, in comparison to PLS3, is that suppression of gene function is, in general, easier to achieve than its activation.

### NCALD Suppression Restores Endocytosis and Synaptic Vesicle Recycling in SMA

To allow rapid and repeated rounds of neurotransmission at the synaptic endplate, synaptic vesicle recycling is essential.[77] In brief, after $Ca^{2+}$-dependent exocytosis and release of acetylcholine (ACh) into the synaptic cleft, the synaptic membrane has to be retrieved rapidly via endocytosis. Then, retrieved vesicular membranes need to be transformed into synaptic vesicles, which are refilled with ACh. These are eventually transported to the readily releasable pool near active zones.[78] Despite the robust fail-safe factor in the motor neuron endplate potential, disturbances in the presynaptic vesicle cycle can severely impact neurotransmission. In SMA, impaired neurotransmission,

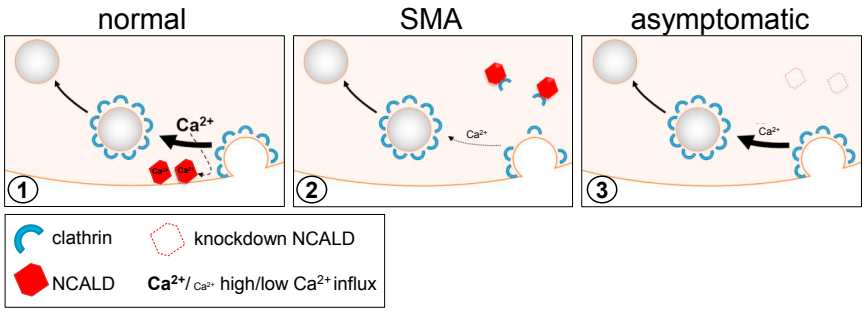


**Figure 7. NCALD Acts as a $Ca^{2+}$-Dependent Regulator of Endocytosis in Synaptic Vesicle Recycling**

Diagrammatic presentation of the mode of action of NCALD in synaptic vesicle recycling in normal, SMA, and asymptomatic pre-synapse of neuronal cells. From left to right: (1) after neurotransmitter release, clathrin binds to empty vesicle membrane causing membrane bending and vesicle formation. High concentration of local $Ca^{2+}$ which is present after vesicle release[85] causes NCALD conformational change and thereby a release of clathrin so that it can perform its function. NCALD may fine-tune recycling speed and help to coordinate proper clathrin coating. (2) In SMA, voltage-dependent $Ca^{2+}$ influx is reduced, decreasing NCALD-clathrin dissociation, thus inhibiting clathrin coating of vesicles. In our model NCALD regulates (increases) the $Ca^{2+}$ dependence of clathrin function. (3) When NCALD level is reduced, the $Ca^{2+}$ dependence is reduced too and even at relatively low intracellular $Ca^{2+}$ levels, clathrin can mediate endocytosis.

disturbed $Ca^{2+}$ homeostasis, decreased synaptic vesicle number, and reduced F-actin caging of reserve pool synaptic vesicles have been reported.[16,69,79,80] For repeated neurotransmitter release, subsequent endocytosis is important;[81] furthermore, endo- and exocytosis are regulated by the $Ca^{2+}$ dynamics within the presynaptic terminals.[82]

We found that low SMN levels cause reduction of voltage-activated $Ca^{2+}$ influx, in accordance with recent studies in a zebrafish SMA model and reported mislocalization of calcium channels in SMA.[83,84] However, unlike SMA pathology, $Ca^{2+}$ influx was not restored by reduced NCALD, suggesting a different counteraction mechanism. Since NCALD interacts with clathrin and actin, two major players in endocytosis,[58,59] we hypothesized that reduced SMN may disturb endocytosis and synaptic vesicle recycling, possibly via decreased $Ca^{2+}$, whereas NCALD knockdown subsequently compensates for SMN loss. We demonstrate in vitro and in ex vivo mouse NMJs that NCALD reduction restores impaired clathrin-dependent endocytosis. Furthermore, chemical endocytosis inhibition in zebrafish caused MN axonogenesis defects that were reversed upon Ncald suppression. Importantly, NCALD binds clathrin only at low $Ca^{2+}$ levels (mimicking unstimulated MNs) but not at high $Ca^{2+}$ levels (mimicking action potentials in MNs). For SMA MNs, with low $Ca^{2+}$ levels even during action potential, we predict that NCALD constantly binds clathrin, thereby inhibiting/reducing its function in synaptic vesicle recycling. However, low NCALD levels, as in asymptomatic individuals, may allow free clathrin to act in endocytosis and synaptic vesicle recycling even at reduced $Ca^{2+}$ levels (Figure 7).

### Implication of NCALD in Other Neurodegenerative Disorders

In agreement with this hypothesis, two other proteins connected to endocytosis cause various forms of SMA. Mutations in *UBA1* (MIM: 314370), an E1 Ubiquitin-Activating Enzyme involved in monoubiquitination which serves as a signal for endocytosis and trafficking of cell surface proteins, has been associated to X-linked SMA (SMAX2 [MIM: 301830]).[86–88] *BICD2* (MIM: 609797), which when mutated causes autosomal-dominant lower-extremity-predominant spinal muscular atrophy-2 (SMALED2 [MIM: 615290]), binds to clathrin heavy chain to promote its transport and augments synaptic vesicle recycling.[89–93] These findings provide additional evidence that disturbances in synaptic vesicle recycling underlie general SMA pathology. Our findings are further strongly supported by data in *C. elegans*, in which disturbed endocytic trafficking at the synaptic level has been reported, and it has been suggested that an increased resistance against infection may explain the high SMA carrier frequency in the population.[71] Moreover, reduced NCALD amount might be beneficial for other MN or neurodegenerative disorders with impaired endocytosis and $Ca^{2+}$ homeostasis, as was shown for Alzheimer disease (AD [MIM: 104300]), where NCALD is highly upregulated,[94] or Parkinson disease (PD [MIM: 168600]), hereditary spastic paraplegia (MIM: PS303350), and ALS (MIM: PS105400), where impaired endocytic trafficking was found.[95] Therefore, it is tempting to speculate that NCALD downregulation might become an efficient strategy against SMA and other neurodegenerative diseases.

## Accession Numbers

All microarray data are available in GEO: GSE58316.

## Supplemental Data

Supplemental Data include seven figures, three tables, and clinical description of Utah family members and can be found with this article online at http://dx.doi.org/10.1016/j.ajhg.2017.01.005.

## Acknowledgments

We thank SMA-affected families, Jay Gopalakrishnan and Natalia Kononenko for critical reading of the manuscript, and CECAD for help with imaging. This work was supported by grants from the Deutsche Forschungsgemeinschaft Wi-945/13-1, Wi-945/14-1, RTG 1970 (B.W.), SMA Europe (M.R.), European Community's Seventh Framework Programme (FP7/2007-2013) under grant agreement no. 2012-305121 "Integrated European -omics research

project for diagnosis and therapy in rare neuromuscular and neurodegenerative diseases (NEUROMICS)" (B.W.), CMMC - C11 (B.W.), IGSDHD (A.K., S.S.), AFM-Telethon (L.T.-B.), and NIH PO1NS066888 (A.C.H.). C.F.B. and F.R. are employees of IONIS Pharmaceuticals. B.W. and M.R. hold an US PCT/EP2014/066276 entitled "Neurocalcin delta inhibitors and therapeutic and non-therapeutic uses thereof" with the international publication number WO/2015/014838 A1.

Received: November 7, 2016
Accepted: January 5, 2017
Published: January 26, 2017

## Web Resources

1000 Genomes, http://www.internationalgenome.org/
Bioconductor, http://www.bioconductor.org
ClinicalTrials.gov, http://clinicaltrials.gov
Cyflogic, http://www.cyflogic.com
ENCODE, https://www.encodeproject.org/
GEO, http://www.ncbi.nlm.nih.gov/geo/
ImageJ, http://rsbweb.nih.gov/ij/
International Mouse Phenotyping Consortium, http://www.mousephenotype.org/data/genes/
LDlink, https://dceg.cancer.gov/tools/analysis/ldlink
Patcher's PowerTools plug-in (WaveMetrics), http://www3.mpibpc.mpg.de/groups/neher/index.php?page=software
R statistical software, http://www.r-project.org/
RefSeq, http://www.ncbi.nlm.nih.gov/RefSeq
UCSC Genome Browser, http://genome.ucsc.edu
UniProt, http://www.uniprot.org/

## References

1. Wirth, B., Garbes, L., and Riessland, M. (2013). How genetic modifiers influence the phenotype of spinal muscular atrophy and suggest future therapeutic approaches. Curr. Opin. Genet. Dev. *23*, 330–338.
2. Kaczmarek, A., Schneider, S., Wirth, B., and Riessland, M. (2015). Investigational therapies for the treatment of spinal muscular atrophy. Expert Opin. Investig. Drugs *24*, 867–881.
3. Lefebvre, S., Bürglen, L., Reboullet, S., Clermont, O., Burlet, P., Viollet, L., Benichou, B., Cruaud, C., Millasseau, P., Zeviani, M., et al. (1995). Identification and characterization of a spinal muscular atrophy-determining gene. Cell *80*, 155–165.
4. Wirth, B. (2000). An update of the mutation spectrum of the survival motor neuron gene (SMN1) in autosomal recessive spinal muscular atrophy (SMA). Hum. Mutat. *15*, 228–237.
5. Liu, Q., Fischer, U., Wang, F., and Dreyfuss, G. (1997). The spinal muscular atrophy disease gene product, SMN, and its associated protein SIP1 are in a complex with spliceosomal snRNP proteins. Cell *90*, 1013–1021.
6. Pellizzoni, L., Kataoka, N., Charroux, B., and Dreyfuss, G. (1998). A novel function for SMN, the spinal muscular atrophy disease gene product, in pre-mRNA splicing. Cell *95*, 615–624.
7. Mourelatos, Z., Dostie, J., Paushkin, S., Sharma, A., Charroux, B., Abel, L., Rappsilber, J., Mann, M., and Dreyfuss, G. (2002). miRNPs: a novel class of ribonucleoproteins containing numerous microRNAs. Genes Dev. *16*, 720–728.
8. Akten, B., Kye, M.J., Hao, T., Wertz, M.H., Singh, S., Nie, D., Huang, J., Merianda, T.T., Twiss, J.L., Beattie, C.E., et al. (2011). Interaction of survival of motor neuron (SMN) and HuD proteins with mRNA cpg15 rescues motor neuron axonal deficits. Proc. Natl. Acad. Sci. USA *108*, 10337–10342.
9. Hsieh-Li, H.M., Chang, J.G., Jong, Y.J., Wu, M.H., Wang, N.M., Tsai, C.H., and Li, H. (2000). A mouse model for spinal muscular atrophy. Nat. Genet. *24*, 66–70.
10. Lorson, C.L., Hahnen, E., Androphy, E.J., and Wirth, B. (1999). A single nucleotide in the SMN gene regulates splicing and is responsible for spinal muscular atrophy. Proc. Natl. Acad. Sci. USA *96*, 6307–6311.
11. Cartegni, L., and Krainer, A.R. (2002). Disruption of an SF2/ASF-dependent exonic splicing enhancer in SMN2 causes spinal muscular atrophy in the absence of SMN1. Nat. Genet. *30*, 377–384.
12. Kashima, T., and Manley, J.L. (2003). A negative element in SMN2 exon 7 inhibits splicing in spinal muscular atrophy. Nat. Genet. *34*, 460–463.
13. Feldkötter, M., Schwarzer, V., Wirth, R., Wienker, T.F., and Wirth, B. (2002). Quantitative analyses of SMN1 and SMN2 based on real-time lightCycler PCR: fast and highly reliable carrier testing and prediction of severity of spinal muscular atrophy. Am. J. Hum. Genet. *70*, 358–368.
14. Lunn, M.R., and Wang, C.H. (2008). Spinal muscular atrophy. Lancet *371*, 2120–2133.
15. Mentis, G.Z., Blivis, D., Liu, W., Drobac, E., Crowder, M.E., Kong, L., Alvarez, F.J., Sumner, C.J., and O'Donovan, M.J. (2011). Early functional impairment of sensory-motor connectivity in a mouse model of spinal muscular atrophy. Neuron *69*, 453–467.
16. Kariya, S., Park, G.H., Maeno-Hikichi, Y., Leykekhman, O., Lutz, C., Arkovitz, M.S., Landmesser, L.T., and Monani, U.R. (2008). Reduced SMN protein impairs maturation of the neuromuscular junctions in mouse models of spinal muscular atrophy. Hum. Mol. Genet. *17*, 2552–2569.
17. Monani, U.R., Sendtner, M., Coovert, D.D., Parsons, D.W., Andreassi, C., Le, T.T., Jablonka, S., Schrank, B., Rossoll, W., Prior, T.W., et al. (2000). The human centromeric survival motor neuron gene (SMN2) rescues embryonic lethality in Smn(-/-) mice and results in a mouse with spinal muscular atrophy. Hum. Mol. Genet. *9*, 333–339.
18. Hamilton, G., and Gillingwater, T.H. (2013). Spinal muscular atrophy: going beyond the motor neuron. Trends Mol. Med. *19*, 40–50.
19. Shababi, M., Feng, Z., Villalon, E., Sibigtroth, C.M., Osman, E.Y., Miller, M.R., Williams-Simon, P.A., Lombardi, A., Sass, T.H., Atkinson, A.K., et al. (2016). Rescue of a mouse model of spinal muscular atrophy with respiratory distress type 1 by AAV9-IGHMBP2 is dose dependent. Mol. Ther. *24*, 855–866.
20. Cobben, J.M., van der Steege, G., Grootscholten, P., de Visser, M., Scheffer, H., and Buys, C.H. (1995). Deletions of the survival motor neuron gene in unaffected siblings of patients with spinal muscular atrophy. Am. J. Hum. Genet. *57*, 805–808.
21. Hahnen, E., Forkert, R., Marke, C., Rudnik-Schöneborn, S., Schönling, J., Zerres, K., and Wirth, B. (1995). Molecular analysis of candidate genes on chromosome 5q13 in autosomal recessive spinal muscular atrophy: evidence of homozygous deletions of the SMN gene in unaffected individuals. Hum. Mol. Genet. *4*, 1927–1933.
22. Wang, C.H., Xu, J., Carter, T.A., Ross, B.M., Dominski, M.K., Bellcross, C.A., Penchaszadeh, G.K., Munsat, T.L., and Gilliam,

T.C. (1996). Characterization of survival motor neuron (SMNT) gene deletions in asymptomatic carriers of spinal muscular atrophy. Hum. Mol. Genet. *5*, 359–365.
23. Prior, T.W., Swoboda, K.J., Scott, H.D., and Hejmanowski, A.Q. (2004). Homozygous SMN1 deletions in unaffected family members and modification of the phenotype by SMN2. Am. J. Med. Genet. A. *130A*, 307–310.
24. Oprea, G.E., Kröber, S., McWhorter, M.L., Rossoll, W., Müller, S., Krawczak, M., Bassell, G.J., Beattie, C.E., and Wirth, B. (2008). Plastin 3 is a protective modifier of autosomal recessive spinal muscular atrophy. Science *320*, 524–527.
25. Heesen, L., Peitz, M., Torres-Benito, L., Hölker, I., Hupperich, K., Dobrindt, K., Jungverdorben, J., Ritzenhofen, S., Weykopf, B., Eckert, D., et al. (2016). Plastin 3 is upregulated in iPSC-derived motoneurons from asymptomatic SMN1-deleted individuals. Cell. Mol. Life Sci. *73*, 2089–2104.
26. Dimitriadi, M., Sleigh, J.N., Walker, A., Chang, H.C., Sen, A., Kalloo, G., Harris, J., Barsby, T., Walsh, M.B., Satterlee, J.S., et al. (2010). Conserved genes act as modifiers of invertebrate SMN loss of function defects. PLoS Genet. *6*, e1001172.
27. Ackermann, B., Kröber, S., Torres-Benito, L., Borgmann, A., Peters, M., Hosseini Barkooie, S.M., Tejero, R., Jakubik, M., Schreml, J., Milbradt, J., et al. (2013). Plastin 3 ameliorates spinal muscular atrophy via delayed axon pruning and improves neuromuscular junction functionality. Hum. Mol. Genet. *22*, 1328–1347.
28. Lotti, F., Imlach, W.L., Saieva, L., Beck, E.S., Hao, T., Li, D.K., Jiao, W., Mentis, G.Z., Beattie, C.E., McCabe, B.D., and Pellizzoni, L. (2012). An SMN-dependent U12 splicing event essential for motor circuit function. Cell *151*, 440–454.
29. Hosseinibarkooie, S., Peters, M., Torres-Benito, L., Rastetter, R.H., Hupperich, K., Hoffmann, A., Mendoza-Ferreira, N., Kaczmarek, A., Janzen, E., Milbradt, J., et al. (2016). The power of human protective modifiers: PLS3 and CORO1C unravel impaired endocytosis in spinal muscular atrophy and rescue SMA phenotype. Am. J. Hum. Genet. *99*, 647–665.
30. Arkblad, E., Tulinius, M., Kroksmark, A.K., Henricsson, M., and Darin, N. (2009). A population-based study of genotypic and phenotypic variability in children with spinal muscular atrophy. Acta Paediatr. *98*, 865–872.
31. Zerres, K., Wirth, B., and Rudnik-Schöneborn, S. (1997). Spinal muscular atrophy–clinical and genetic correlations. Neuromuscul. Disord. *7*, 202–207.
32. Sun, Y., Grimmler, M., Schwarzer, V., Schoenen, F., Fischer, U., and Wirth, B. (2005). Molecular and functional analysis of intragenic SMN1 mutations in patients with spinal muscular atrophy. Hum. Mutat. *25*, 64–71.
33. Gudbjartsson, D.F., Jonasson, K., Frigge, M.L., and Kong, A. (2000). Allegro, a new computer program for multipoint linkage analysis. Nat. Genet. *25*, 12–13.
34. Thiele, H., and Nürnberg, P. (2005). HaploPainter: a tool for drawing pedigrees with complex haplotypes. Bioinformatics *21*, 1730–1732.
35. Rüschendorf, F., and Nürnberg, P. (2005). ALOHOMORA: a tool for linkage analysis using 10K SNP array data. Bioinformatics *21*, 2123–2125.
36. Dunning, M.J., Barbosa-Morais, N.L., Lynch, A.G., Tavaré, S., and Ritchie, M.E. (2008). Statistical issues in the analysis of Illumina data. BMC Bioinformatics *9*, 85.
37. Huber, W., von Heydebreck, A., Sültmann, H., Poustka, A., and Vingron, M. (2002). Variance stabilization applied to microarray data calibration and to the quantification of differential expression. Bioinformatics *18* (*Suppl 1*), S96–S104.
38. Wettenhall, J.M., and Smyth, G.K. (2004). limmaGUI: a graphical user interface for linear modeling of microarray data. Bioinformatics *20*, 3705–3706.
39. Benjamini, Y., and Hochberg, Y. (1995). Controlling the false discovery rate: a practical and powerful approach to multiple testing. J.R. Stat. Soc. *57*, 289–300.
40. Flanagan-Steet, H., Fox, M.A., Meyer, D., and Sanes, J.R. (2005). Neuromuscular synapses can form in vivo by incorporation of initially aneural postsynaptic specializations. Development *132*, 4471–4481.
41. Briese, M., Esmaeili, B., Fraboulet, S., Burt, E.C., Christodoulou, S., Towers, P.R., Davies, K.E., and Sattelle, D.B. (2009). Deletion of smn-1, the *Caenorhabditis elegans* ortholog of the spinal muscular atrophy gene, results in locomotor dysfunction and reduced lifespan. Hum. Mol. Genet. *18*, 97–104.
42. Calixto, A., Chelur, D., Topalidou, I., Chen, X., and Chalfie, M. (2010). Enhanced neuronal RNAi in *C. elegans* using SID-1. Nat. Methods *7*, 554–559.
43. Riessland, M., Ackermann, B., Förster, A., Jakubik, M., Hauke, J., Garbes, L., Fritzsche, I., Mende, Y., Blumcke, I., Hahnen, E., and Wirth, B. (2010). SAHA ameliorates the SMA phenotype in two mouse models for spinal muscular atrophy. Hum. Mol. Genet. *19*, 1492–1506.
44. El-Khodor, B.F., Edgar, N., Chen, A., Winberg, M.L., Joyce, C., Brunner, D., Suárez-Fariñas, M., and Heyes, M.P. (2008). Identification of a battery of tests for drug candidate evaluation in the SMNDelta7 neonate model of spinal muscular atrophy. Exp. Neurol. *212*, 29–43.
45. Bogdanik, L.P., Osborne, M.A., Davis, C., Martin, W.P., Austin, A., Rigo, F., Bennett, C.F., and Lutz, C.M. (2015). Systemic, postsymptomatic antisense oligonucleotide rescues motor unit maturation delay in a new mouse model for type II/III spinal muscular atrophy. Proc. Natl. Acad. Sci. USA *112*, E5863–E5872.
46. Greene, L.A., and Tischler, A.S. (1976). Establishment of a noradrenergic clonal line of rat adrenal pheochromocytoma cells which respond to nerve growth factor. Proc. Natl. Acad. Sci. USA *73*, 2424–2428.
47. Armstrong, C.M., and Bezanilla, F. (1974). Charge movement associated with the opening and closing of the activation gates of the Na channels. J. Gen. Physiol. *63*, 533–552.
48. Dubowitz, V. (1999). Very severe spinal muscular atrophy (SMA type 0): an expanding clinical phenotype. Eur. J. Paediatr. Neurol. *3*, 49–51.
49. Sugarman, E.A., Nagan, N., Zhu, H., Akmaev, V.R., Zhou, Z., Rohlfs, E.M., Flynn, K., Hendrickson, B.C., Scholl, T., Sirko-Osadsa, D.A., and Allitto, B.A. (2012). Pan-ethnic carrier screening and prenatal diagnosis for spinal muscular atrophy: clinical laboratory analysis of >72,400 specimens. Eur. J. Hum. Genet. *20*, 27–32.
50. Burgoyne, R.D., and Haynes, L.P. (2012). Understanding the physiological roles of the neuronal calcium sensor proteins. Mol. Brain *5*, 2.
51. Di Sole, F., Vadnagara, K., Moe, O.W., and Babich, V. (2012). Calcineurin homologous protein: a multifunctional Ca2+-binding protein family. Am. J. Physiol. Renal Physiol. *303*, F165–F179.
52. Ladant, D. (1995). Calcium and membrane binding properties of bovine neurocalcin delta expressed in *Escherichia coli*. J. Biol. Chem. *270*, 3179–3185.

53. Hidaka, H., and Okazaki, K. (1993). Neurocalcin family: a novel calcium-binding protein abundant in bovine central nervous system. Neurosci. Res. *16*, 73–77.
54. Viviano, J., Krishnan, A., Wu, H., and Venkataraman, V. (2016). Data on the calcium-induced mobility shift of myristoylated and non-myristoylated forms of neurocalcin delta. Data Brief *7*, 630–633.
55. Iino, S., Kobayashi, S., and Hidaka, H. (1998). Neurocalcin-immunopositive nerve terminals in the muscle spindle, Golgi tendon organ and motor endplate. Brain Res. *808*, 294–299.
56. Yamatani, H., Kawasaki, T., Mita, S., Inagaki, N., and Hirata, T. (2010). Proteomics analysis of the temporal changes in axonal proteins during maturation. Dev. Neurobiol. *70*, 523–537.
57. Venkataraman, V., Duda, T., Ravichandran, S., and Sharma, R.K. (2008). Neurocalcin delta modulation of ROS-GC1, a new model of Ca(2+) signaling. Biochemistry *47*, 6590–6601.
58. Ivings, L., Pennington, S.R., Jenkins, R., Weiss, J.L., and Burgoyne, R.D. (2002). Identification of Ca2+-dependent binding partners for the neuronal calcium sensor protein neurocalcin delta: interaction with actin, clathrin and tubulin. Biochem. J. *363*, 599–608.
59. Haucke, V., Neher, E., and Sigrist, S.J. (2011). Protein scaffolds in the coupling of synaptic exocytosis and endocytosis. Nat. Rev. Neurosci. *12*, 127–138.
60. Cashman, N.R., Durham, H.D., Blusztajn, J.K., Oda, K., Tabira, T., Shaw, I.T., Dahrouge, S., and Antel, J.P. (1992). Neuroblastoma x spinal cord (NSC) hybrid cell lines resemble developing motor neurons. Dev. Dyn. *194*, 209–221.
61. Rossoll, W., Jablonka, S., Andreassi, C., Kröning, A.K., Karle, K., Monani, U.R., and Sendtner, M. (2003). Smn, the spinal muscular atrophy-determining gene product, modulates axon growth and localization of beta-actin mRNA in growth cones of motoneurons. J. Cell Biol. *163*, 801–812.
62. McWhorter, M.L., Monani, U.R., Burghes, A.H., and Beattie, C.E. (2003). Knockdown of the survival motor neuron (Smn) protein in zebrafish causes defects in motor axon outgrowth and pathfinding. J. Cell Biol. *162*, 919–931.
63. Drapeau, P., Buss, R.R., Ali, D.W., Legendre, P., and Rotundo, R.L. (2001). Limits to the development of fast neuromuscular transmission in zebrafish. J. Neurophysiol. *86*, 2951–2956.
64. Westerfield, M., McMurray, J.V., and Eisen, J.S. (1986). Identified motoneurons and their innervation of axial muscles in the zebrafish. J. Neurosci. *6*, 2267–2277.
65. Fatt, P., and Katz, B. (1951). An analysis of the end-plate potential recorded with an intracellular electrode. J. Physiol. *115*, 320–370.
66. Gomez, M., De Castro, E., Guarin, E., Sasakura, H., Kuhara, A., Mori, I., Bartfai, T., Bargmann, C.I., and Nef, P. (2001). Ca2+ signaling via the neuronal calcium sensor-1 regulates associative learning and memory in *C. elegans*. Neuron *30*, 241–248.
67. Somers, E., Riessland, M., Schreml, J., Wirth, B., Gillingwater, T.H., and Parson, S.H. (2013). Increasing SMN levels using the histone deacetylase inhibitor SAHA ameliorates defects in skeletal muscle microvasculature in a mouse model of severe spinal muscular atrophy. Neurosci. Lett. *544*, 100–104.
68. Hua, Y., Sahashi, K., Rigo, F., Hung, G., Horev, G., Bennett, C.F., and Krainer, A.R. (2011). Peripheral SMN restoration is essential for long-term rescue of a severe spinal muscular atrophy mouse model. Nature *478*, 123–126.
69. Ruiz, R., Casañas, J.J., Torres-Benito, L., Cano, R., and Tabares, L. (2010). Altered intracellular Ca2+ homeostasis in nerve terminals of severe spinal muscular atrophy mice. J. Neurosci. *30*, 849–857.
70. Kübler, E., and Riezman, H. (1993). Actin and fimbrin are required for the internalization step of endocytosis in yeast. EMBO J. *12*, 2855–2862.
71. Dimitriadi, M., Derdowski, A., Kalloo, G., Maginnis, M.S., O'Hern, P., Bliska, B., Sorkaç, A., Nguyen, K.C., Cook, S.J., Poulogiannis, G., et al. (2016). Decreased function of survival motor neuron protein impairs endocytic pathways. Proc. Natl. Acad. Sci. USA *113*, E4377–E4386.
72. von Kleist, L., Stahlschmidt, W., Bulut, H., Gromova, K., Puchkov, D., Robertson, M.J., MacGregor, K.A., Tomilin, N., Pechstein, A., Chau, N., et al. (2011). Role of the clathrin terminal domain in regulating coated pit dynamics revealed by small molecule inhibition. Cell *146*, 471–484.
73. Macia, E., Ehrlich, M., Massol, R., Boucrot, E., Brunner, C., and Kirchhausen, T. (2006). Dynasore, a cell-permeable inhibitor of dynamin. Dev. Cell *10*, 839–850.
74. Wirth, B., Barkats, M., Martinat, C., Sendtner, M., and Gillingwater, T.H. (2015). Moving towards treatments for spinal muscular atrophy: hopes and limits. Expert Opin. Emerg. Drugs *20*, 353–356.
75. Benkhelifa-Ziyyat, S., Besse, A., Roda, M., Duque, S., Astord, S., Carcenac, R., Marais, T., and Barkats, M. (2013). Intramuscular scAAV9-SMN injection mediates widespread gene delivery to the spinal cord and decreases disease severity in SMA mice. Mol. Ther. *21*, 282–290.
76. Shababi, M., Lorson, C.L., and Rudnik-Schöneborn, S.S. (2014). Spinal muscular atrophy: a motor neuron disorder or a multi-organ disease? J. Anat. *224*, 15–28.
77. Sudhof, T.C. (2004). The synaptic vesicle cycle. Annu. Rev. Neurosci. *27*, 509–547.
78. Parsons, R.L., Calupca, M.A., Merriam, L.A., and Prior, C. (1999). Empty synaptic vesicles recycle and undergo exocytosis at vesamicol-treated motor nerve terminals. J. Neurophysiol. *81*, 2696–2700.
79. Kong, L., Wang, X., Choe, D.W., Polley, M., Burnett, B.G., Bosch-Marcé, M., Griffin, J.W., Rich, M.M., and Sumner, C.J. (2009). Impaired synaptic vesicle release and immaturity of neuromuscular junctions in spinal muscular atrophy mice. J. Neurosci. *29*, 842–851.
80. Murray, L.M., Comley, L.H., Thomson, D., Parkinson, N., Talbot, K., and Gillingwater, T.H. (2008). Selective vulnerability of motor neurons and dissociation of pre- and post-synaptic pathology at the neuromuscular junction in mouse models of spinal muscular atrophy. Hum. Mol. Genet. *17*, 949–962.
81. Stevens, C.F. (2003). Neurotransmitter release at central synapses. Neuron *40*, 381–388.
82. Südhof, T.C. (2012). Calcium control of neurotransmitter release. Cold Spring Harb. Perspect. Biol. *4*, a011353.
83. Jablonka, S., Beck, M., Lechner, B.D., Mayer, C., and Sendtner, M. (2007). Defective Ca2+ channel clustering in axon terminals disturbs excitability in motoneurons in spinal muscular atrophy. J. Cell Biol. *179*, 139–149.
84. See, K., Yadav, P., Giegerich, M., Cheong, P.S., Graf, M., Vyas, H., Lee, S.G., Mathavan, S., Fischer, U., Sendtner, M., and Winkler, C. (2014). SMN deficiency alters Nrxn2 expression and splicing in zebrafish and mouse models of spinal muscular atrophy. Hum. Mol. Genet. *23*, 1754–1770.
85. Burgoyne, R.D., and Morgan, A. (2003). Secretory granule exocytosis. Physiol. Rev. *83*, 581–632.

86. Wishart, T.M., Mutsaers, C.A., Riessland, M., Reimer, M.M., Hunter, G., Hannam, M.L., Eaton, S.L., Fuller, H.R., Roche, S.L., Somers, E., et al. (2014). Dysregulation of ubiquitin homeostasis and β-catenin signaling promote spinal muscular atrophy. J. Clin. Invest. *124*, 1821–1834.
87. Mukhopadhyay, D., and Riezman, H. (2007). Proteasome-independent functions of ubiquitin in endocytosis and signaling. Science *315*, 201–205.
88. Ramser, J., Ahearn, M.E., Lenski, C., Yariz, K.O., Hellebrand, H., von Rhein, M., Clark, R.D., Schmutzler, R.K., Lichtner, P., Hoffman, E.P., et al. (2008). Rare missense and synonymous variants in UBE1 are associated with X-linked infantile spinal muscular atrophy. Am. J. Hum. Genet. *82*, 188–193.
89. Li, X., Kuromi, H., Briggs, L., Green, D.B., Rocha, J.J., Sweeney, S.T., and Bullock, S.L. (2010). Bicaudal-D binds clathrin heavy chain to promote its transport and augments synaptic vesicle recycling. EMBO J. *29*, 992–1006.
90. Neveling, K., Martinez-Carrera, L.A., Hölker, I., Heister, A., Verrips, A., Hosseini-Barkooie, S.M., Gilissen, C., Vermeer, S., Pennings, M., Meijer, R., et al. (2013). Mutations in BICD2, which encodes a golgin and important motor adaptor, cause congenital autosomal-dominant spinal muscular atrophy. Am. J. Hum. Genet. *92*, 946–954.
91. Oates, E.C., Rossor, A.M., Hafezparast, M., Gonzalez, M., Speziani, F., MacArthur, D.G., Lek, M., Cottenie, E., Scoto, M., Foley, A.R., et al.; UK10K (2013). Mutations in BICD2 cause dominant congenital spinal muscular atrophy and hereditary spastic paraplegia. Am. J. Hum. Genet. *92*, 965–973.
92. Peeters, K., Litvinenko, I., Asselbergh, B., Almeida-Souza, L., Chamova, T., Geuens, T., Ydens, E., Zimoń, M., Irobi, J., De Vriendt, E., et al. (2013). Molecular defects in the motor adaptor BICD2 cause proximal spinal muscular atrophy with autosomal-dominant inheritance. Am. J. Hum. Genet. *92*, 955–964.
93. Martinez-Carrera, L.A., and Wirth, B. (2015). Dominant spinal muscular atrophy is caused by mutations in BICD2, an important golgin protein. Front. Neurosci. *9*, 401.
94. Suszyńska-Zajczyk, J., Luczak, M., Marczak, L., and Jakubowski, H. (2014). Hyperhomocysteinemia and bleomycin hydrolase modulate the expression of mouse brain proteins involved in neurodegeneration. J. Alzheimers Dis. *40*, 713–726.
95. Schreij, A.M., Fon, E.A., and McPherson, P.S. (2016). Endocytic membrane trafficking and neurodegenerative disease. Cell. Mol. Life Sci. *73*, 1529–1545.

**The American Journal of Human Genetics, Volume *100***

## Supplemental Data

# Neurocalcin Delta Suppression Protects against Spinal Muscular Atrophy in Humans and across Species by Restoring Impaired Endocytosis

**Markus Riessland, Anna Kaczmarek, Svenja Schneider, Kathryn J. Swoboda, Heiko Löhr, Cathleen Bradler, Vanessa Grysko, Maria Dimitriadi, Seyyedmohsen Hosseinibarkooie, Laura Torres-Benito, Miriam Peters, Aaradhita Upadhyay, Nasim Biglari, Sandra Kröber, Irmgard Hölker, Lutz Garbes, Christian Gilissen, Alexander Hoischen, Gudrun Nürnberg, Peter Nürnberg, Michael Walter, Frank Rigo, C. Frank Bennett, Min Jeong Kye, Anne C. Hart, Matthias Hammerschmidt, Peter Kloppenburg, and Brunhilde Wirth**

**SUPPLEMENTAL CASE REPORTS**

**Clinical Investigation of SMA Patients and Asymptomatic Family Members of the Utah Family.**

Informed written consent (or parental consent and assent where appropriate) was obtained from all participating family members under University of Utah Institutional Review Board Protocol #8751 entitled Clinical and Genetics Studies in Spinal Muscular Atrophy. DNA was extracted from whole blood samples using routine protocols in all subjects; skin biopsies for fibroblast cultures were performed on a subset of individuals. All individuals with homozygous SMN deletion agreed to participate in additional detailed clinical investigations, including a full physical and neurological examination, electrophysiologic investigations inclusive of maximum ulnar compound muscle action potential amplitudes (CMAP) and motor unit number estimation (MUNE) to assess peripheral motor nerve function (using Vikingquest electromyography system, Natus and previously published protocol www.smaoutcomes.org, (Swoboda et al., 2005); dual energy X-ray absorptiometry (DEXA) scans to assess whole body composition and bone density (XR-26 system, Norland Corporation, Fort Atkinson, Wisconsin). A summary of phenotypes and investigations for *SMN1* deleted individuals is detailed below. History of evolution of clinical symptoms is additionally provided for the proband, 9164 and affected sister 9994 with SMA type I.

The proband was a female infant (**Figure 1A**, IV-2, SMA-I, 0 *SMN1*, 2 *SMN2* copies) born full-term following an uneventful pregnancy and delivery. In retrospect, parents noted hypotonia from about 2 weeks of age. Neurologic evaluation at age 3.8 months revealed generalized weakness and hypotonia, absent head control, areflexia and paradoxical breathing indicating intercostal muscle weakness. She had limited antigravity proximal limb movements. Ulnar CMAP was already significantly diminished: 0.9 mV (normal > 5 mV) and MUNE 8 (normal > 150). She received nocturnal noninvasive ventilatory support with bilevel respiratory support (BIPAP) from age 5.5 months. Nasogastric tube was required from 7 months and she received gastrostomy tube at 8.7 months. DEXA scan performed at 12 months of age revealed severely

diminished fat-free lean body mass for age. She died of respiratory failure at 3 years of age when her ventilator was inadvertently unplugged.

Unaffected brother (**Figure 1A**, IV-3, asymptomatic, 0 *SMN1*, 4 *SMN2* copies) was born full-term following an uneventful pregnancy, BW 6 lbs 14 oz. Prenatal diagnosis via amniocentesis was performed prior to the delivery. He was examined and followed closely prospectively from birth. Neurologic examination at 2 weeks, and 2, 3, 6, 9 and 12 months was normal. He sat by six months, stood by 9 months and walked independently by 10 months. CMAP was initially 3.8 mV at 2 weeks of age and progressively increased over the ensuing months, to reach a maximum of ~9 mV by 9 months of age. MUNE values were normal, and DEXA scan revealed normal body composition. He was evaluated on a yearly basis, and continued to develop normally. At 13 years of age, his neurologic exam is entirely normal; he can perform 20 squats without difficulty and he is normally active for age. He demonstrates a squint when going from dark to bright environments.

Unaffected brother (**Figure 1A**, IV-4, asymptomatic, 0 *SMN1*, 4 *SMN2* copies) was born full-term following an uneventful pregnancy and delivery, birth weight 8 lbs 2 oz. Examination at 1 day of age was normal. Detailed investigations performed at 3 months of age revealed normal CMAP (10.3 mV) and MUNE (~150) values. Developmental proceeded normally; he sat by 6 months and walked by 12 months. DEXA at 8 months demonstrated normal body composition. He demonstrated some modest speech delay, and was a bit clumsy but neurologic examination remained normal. At 11 years of age, he remains neurologically normal. He is normally active and can do 20 squats without evident difficulty or fatigue. He is photosensitive, with a prominent squint when going from dim to bright environment; this is especially notable in family photos taken outdoors.

Affected sister (**Figure 1A**, IV-5, SMA-I, 0 *SMN1*, 2 *SMN2*) was born 10 days post-term via induced vaginal delivery. At day 1 of life, she appeared clinically normal. However, by 4 days of age, she was hypotonic, with reduced spontaneous voluntary limb movements and evident tongue fasciculation. She was areflexic but still had good suck, cry and head control and

proximal antigravity limb movements. She had bilateral wrist drop and poor coloration of distal extremities. CMAP at 4 days of age was low (2.7 mV) and fell precipitously to 0.8 mV by 3 weeks of age, indicating rapidly progressive distal denervation. She received Nissan and gastrostomy-tube surgery at six weeks of age, and was on nocturnal BIPAP support by 3 months of age. She had numerous hospitalizations in the first year for acute on chronic respiratory failure, usually in the setting of apparent viral infections, including respiratory syncytial virus. She underwent tracheostomy at 22 months of age for increasing respiratory instability; however, support was withdrawn at 5 years of age after a critical illness with sepsis and multi-organ failure.

Unaffected father (**Figure 1A**, III-1, asymptomatic, 0 SMN1, 4 *SMN2* copies) underwent detailed clinical investigation at 30 years of age, when carrier testing indicated an apparent homozygous SMN1 deletion. Detailed neurologic examination was entirely normal. Maximum ulnar CMAP (11.3 mV) and MUNE (150) values were normal. Whole body DEXA scan indicated normal body composition. He remains clinically unaffected at 43 years of age, without evidence of proximal muscle weakness or fatigability. He admits to photosensitivity, wears sunglasses most days, and has a characteristic squint in photos taken outdoors.

Unaffected paternal uncle (**Figure 1A**, III-4, asymptomatic, 0 *SMN1*, 4 *SMN2* copies) underwent detailed clinical investigation at 25 years of age. Detailed neurologic examination was normal, with no evident weakness or fatigability. Maximum ulnar CMAP (14.9 mV) and MUNE (160) values were normal. DEXA indicated normal body composition. At 37 years of age, he remains clinically asymptomatic. He was not examined for clinically evident photosensitivity.

Unaffected paternal aunt (**Figure 1A**, III-6, asymptomatic, 0 *SMN1*, 4 *SMN2* copies) underwent detailed clinical investigation at 22 years of age. Neurologic examination was normal, without evident weakness or fatigability. Maximum ulnar CMAP (10.6) and MUNE (160) values were normal. DEXA indicated normal body composition. At 35 years of age, she remains clinically asymptomatic. She was not examined for clinically evident photosensitivity.

## SUPPLEMENTAL FIGURES AND LEGENDS

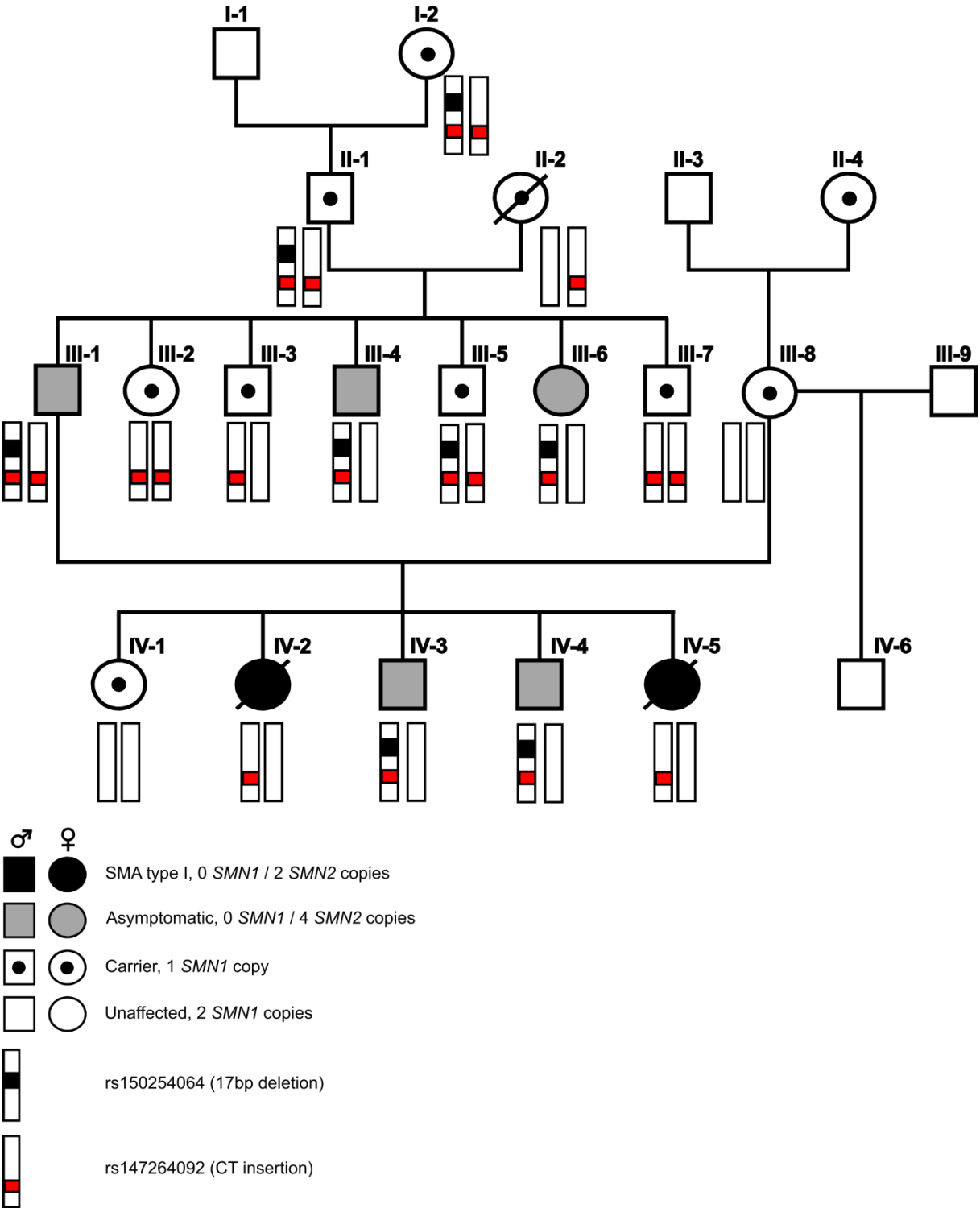


**Figure S1** Pedigree showing of Utah family segregation of identified variants**.** (CT insertion in intron1 of *NCALD* and 17 bp deletion upstream of *NCALD*) on chromosome 8.

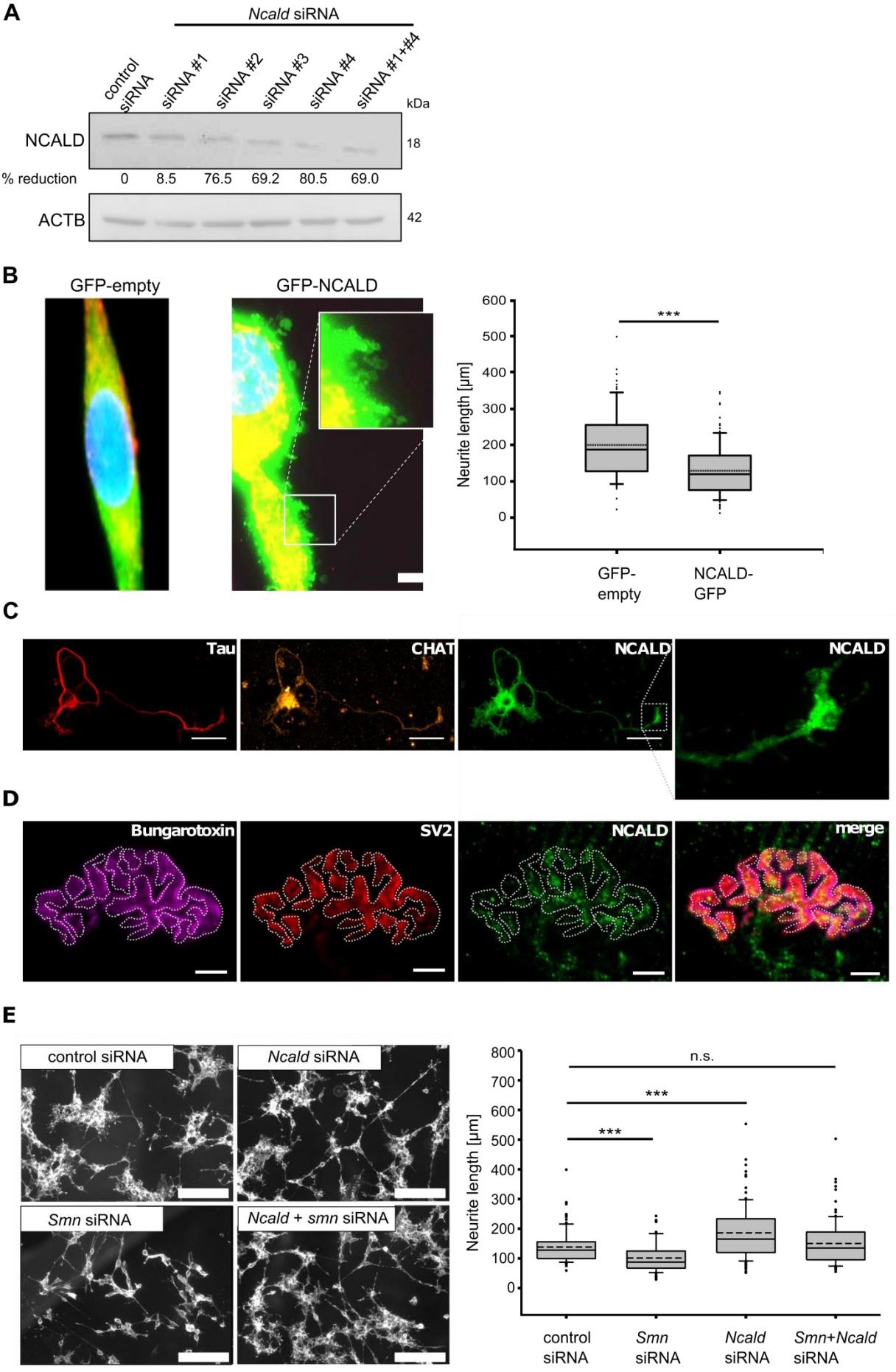
A
Ncald siRNA
control siRNA
siRNA #1
siRNA #2
siRNA #3
siRNA #4
siRNA #1+#4
kDa
NCALD
18
% reduction
0
8.5
76.5
69.2
80.5
69.0
ACTB
42
B
GFP-empty
GFP-NCALD
Neurite length [µm]
***
GFP-empty
NCALD-GFP
C
Tau
CHAT
NCALD
NCALD
D
Bungarotoxin
SV2
NCALD
merge
E
control siRNA
Ncald siRNA
Smn siRNA
Ncald + smn siRNA
Neurite length [µm]
n.s.
***
***
control siRNA
Smn siRNA
Ncald siRNA
Smn+Ncald siRNA

**Figure S2. NCALD Downregulation Restores Neurite Outgrowth in SMN-Deficient Neuronal Cells, NCALD Overexpression Induces Membrane Blebbing.**

(A) WB verifying NCALD reduction upon siRNA treatment 72h post transfection. 4 different siRNAs were tested; for all further experiments siNcald #2 was used. Numbers below NCALD blot indicate quantified percentage of knockdown efficiency.

(B) Representative image of an NSC34 cell overexpressing GFP or NCALD-GFP. Significant membrane blebbing is present only in the NCALD-GFP overexpressing cell. Inset shows detail of membrane blebbing. Scale bar, 10 µm. Quantification of neurite outgrowth length of NSC34 cells transfected either with GFP or NCALD-GFP and treated with 1µm RA for 3 days and stained with Phalloidin-rhodamine. NCALD-GFP cells showed reduced neurite length. N = 100; ***P < 0.001.

(C) Representative images of primary murine MNs cultured 6 days *in vitro* (DIV) stained with antibodies against NCALD, Tau (axon–specific marker) and CHAT (MN-specific marker). Note the high expression of NCALD in soma and growth cones (inset). Scale bar, 50 µm.

(D) Exemplary NCALD staining of NMJ in TVA of 3-week-old wt mice. Postsynaptic terminals stained with Bungarotoxin (magenta) and presynaptic terminals with SV2 (red, delineated by the dashed line). NCALD (green) localizes to presynaptic region, based on overlap between SV2 and NCALD, by Pearson`s correlation of 0.72 ± 0.082 (Z stack, 0.5 µm per stack; N = 4). Scale bar, 5 µm.

(E) Representative images and quantification of neurite outgrowth of NSC34 cells treated with respective siRNAs (50nm) and differentiated with retinoic acid (1µM RA). 4 days after siRNA transfection and 3 days after RA treatment *Smn* siRNA cells showed neurite outgrowth defects. *Smn+Ncald* siRNA cells showed a phenotype rescue and an outgrowth comparable to control siRNA cells. Cells were stained with Phalloidin-Alexa Fluor 568. Scale bar, 200 µm. N = 100 cells per treatment; ***P <0.001; dashed line = mean (control siRNA: 138.32 µm; *Smn* siRNA: 101.35µm; *Ncald* siRNA: 185.9 µm; *Smn+Ncald* siRNA: 150.36 µm), line=median (control siRNA: 122.5 µm; *Smn* siRNA: 87.5 µm; *Ncald* siRNA: 165 µm; *Smn+Ncald* siRNA: 135 µm).

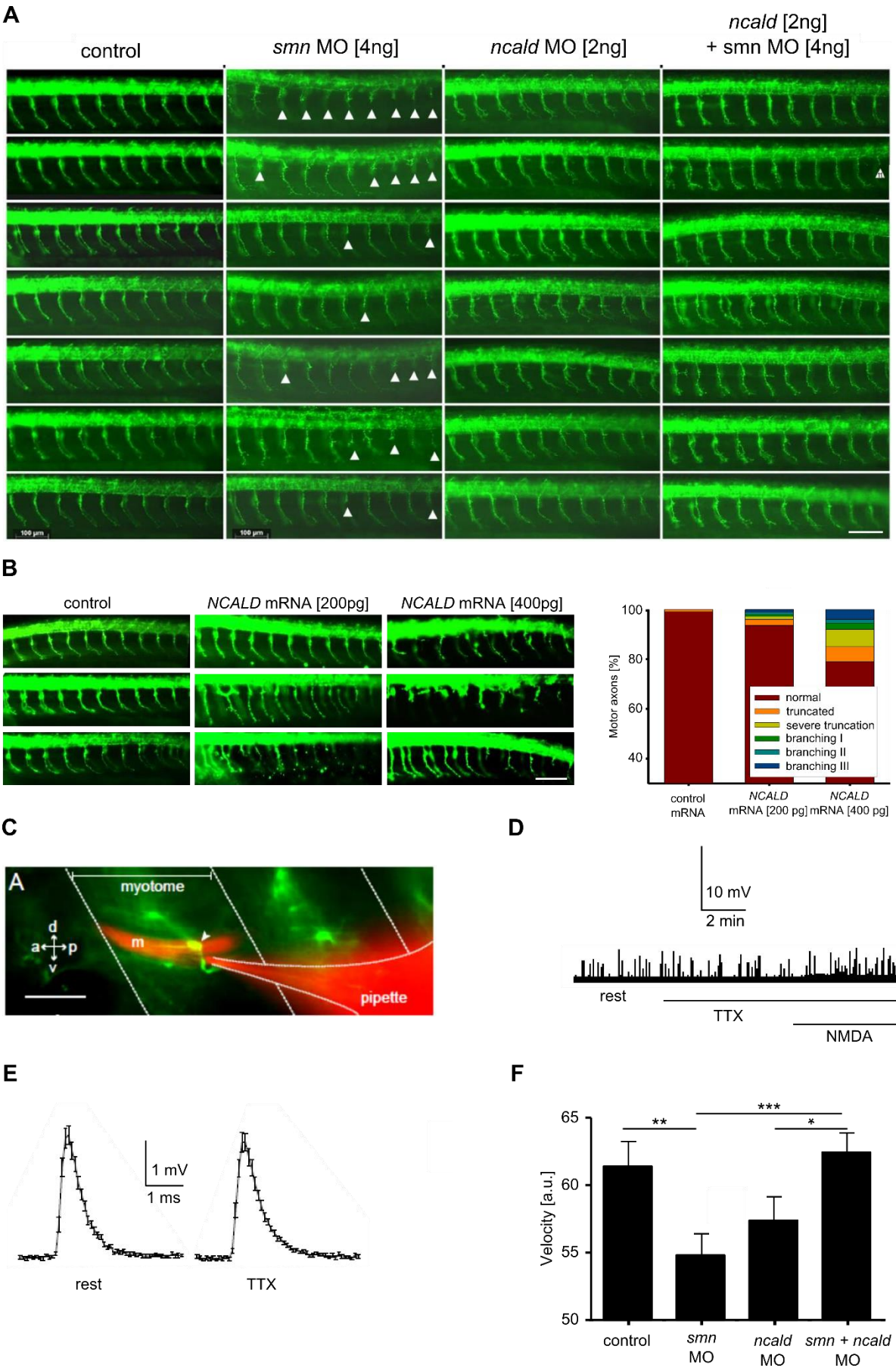
A
control
smn MO [4ng]
ncald MO [2ng]
ncald [2ng]
+ smn MO [4ng]
B
control
NCALD mRNA [200pg]
NCALD mRNA [400pg]
Motor axons [%]
100
80
60
40
normal
truncated
severe truncation
branching I
branching II
branching III
control mRNA
NCALD mRNA [200 pg]
NCALD mRNA [400 pg]
C
A
myotome
d
a
p
v
m
pipette
D
10 mV
2 min
rest
TTX
NMDA
E
1 mV
1 ms
rest
TTX
F
Velocity [a.u.]
65
60
55
50
**
***
*
control
smn MO
ncald MO
smn + ncald MO

**Figure S3. Overview of Motor Neuron Phenotype after Downregulation or Overexpression of NCALD and Characterization of Electrophysiological Properties of Zebrafish Muscles and Swimming Behavior of Zebrafish**

(A) Representative overview of motor axon outgrowth phenotype of 34 hpf morphants (including pictures from main Figure 3). Significant truncation phenotype of *smn* morphants is corrected by additional *ncald* KD. Scale bar, 100 µm.

(B) Representative overview of motor axon outgrowth phenotype of 34 hpf zebrafish after human *NCALD* mRNA injection. Quantification shows the dose-dependent truncation phenotype of zebrafish overexpressing NCALD. Scale bar, 100µm. First 10 motor axons posterior to the yolk were evaluated in every fish. n ≥200 motor axons per mRNA injection.

(C) Fluorescence image of the recording situation. A wild-type ventral fast muscle cell was filled with rhodamine dextran (red) during a whole-cell patch-clamp recording. The muscle cell (m) is innervated by GFP-labeled motor neurons (green) indicated by the arrowhead. The muscle cell spans one myotome. Scale bar, 20 µm.

(D) Whole-cell current clamp recordings of zebrafish muscles. Diagram shows original whole-cell current clamp recordings of mEPPs: at rest, during 1 µM TTX, -and during simultaneous TTX- and 100 µM NMDA-application. NMDA application failed to increase muscle action potentials in the presence of TTX. mEEP amplitude and frequency are not TTX-sensitive.

(E) Means of 30 EPPs in the absence or presence of 1 µM TTX.

(F) Bar graph of high-speed camera swimming velocity measurement of 48 hpf zebrafish embryos (N = 30 per treatment). After LoLitracker software evaluation, mean swimming velocity is given in arbitrary units.

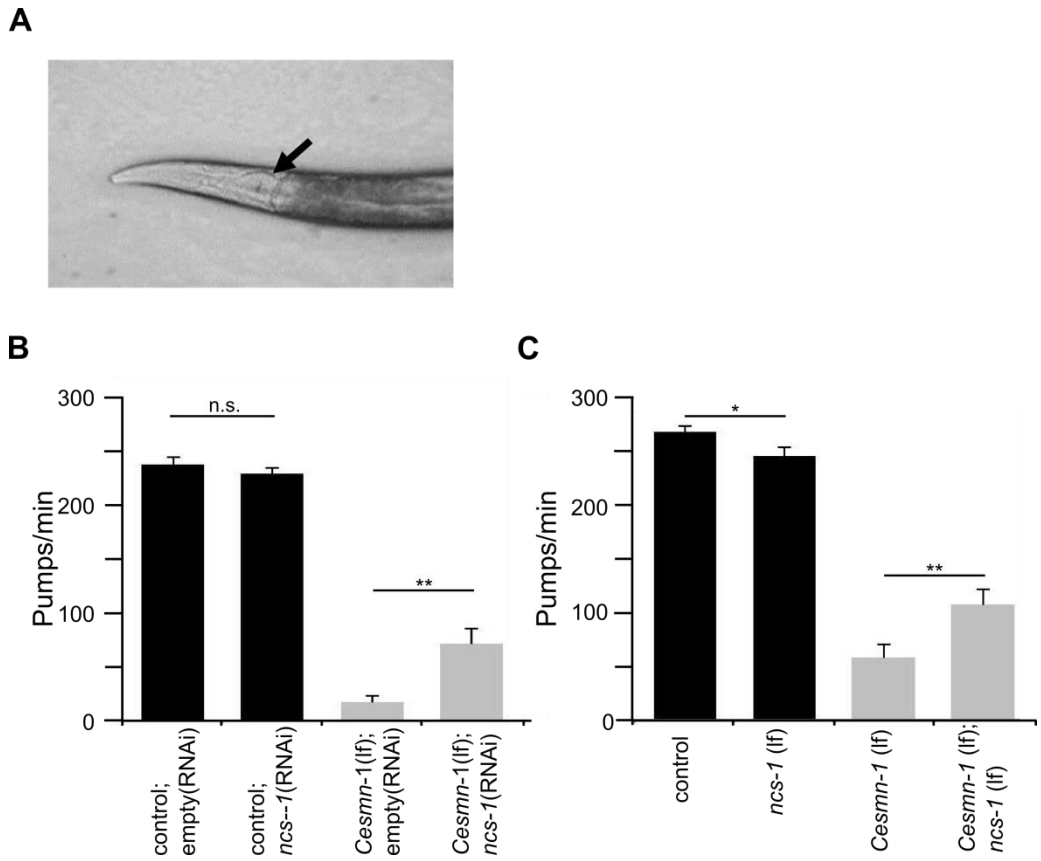


**Figure S4. *Nsc-1* (*ncald* Ortholog) Reduction Corrects the Phenotype in *C. elegans***

(A) *C. elegans* neuromuscular function was assessed based on pharyngeal pumping rates during feeding. Arrow indicates the pharyngeal grinder, which moves during each pumping event.

(B, C) Quantification of pharyngeal pumping in wild type or mutant *smn-1* worms fed with control or *ncs-1* RNAi knockdown (I) or with an *ncs-1(qa401)* mutant allele (J). For every determination n ≥25. Mean ± SEM is shown; * P ≤ 0.05, ** P ≤ 0.01.

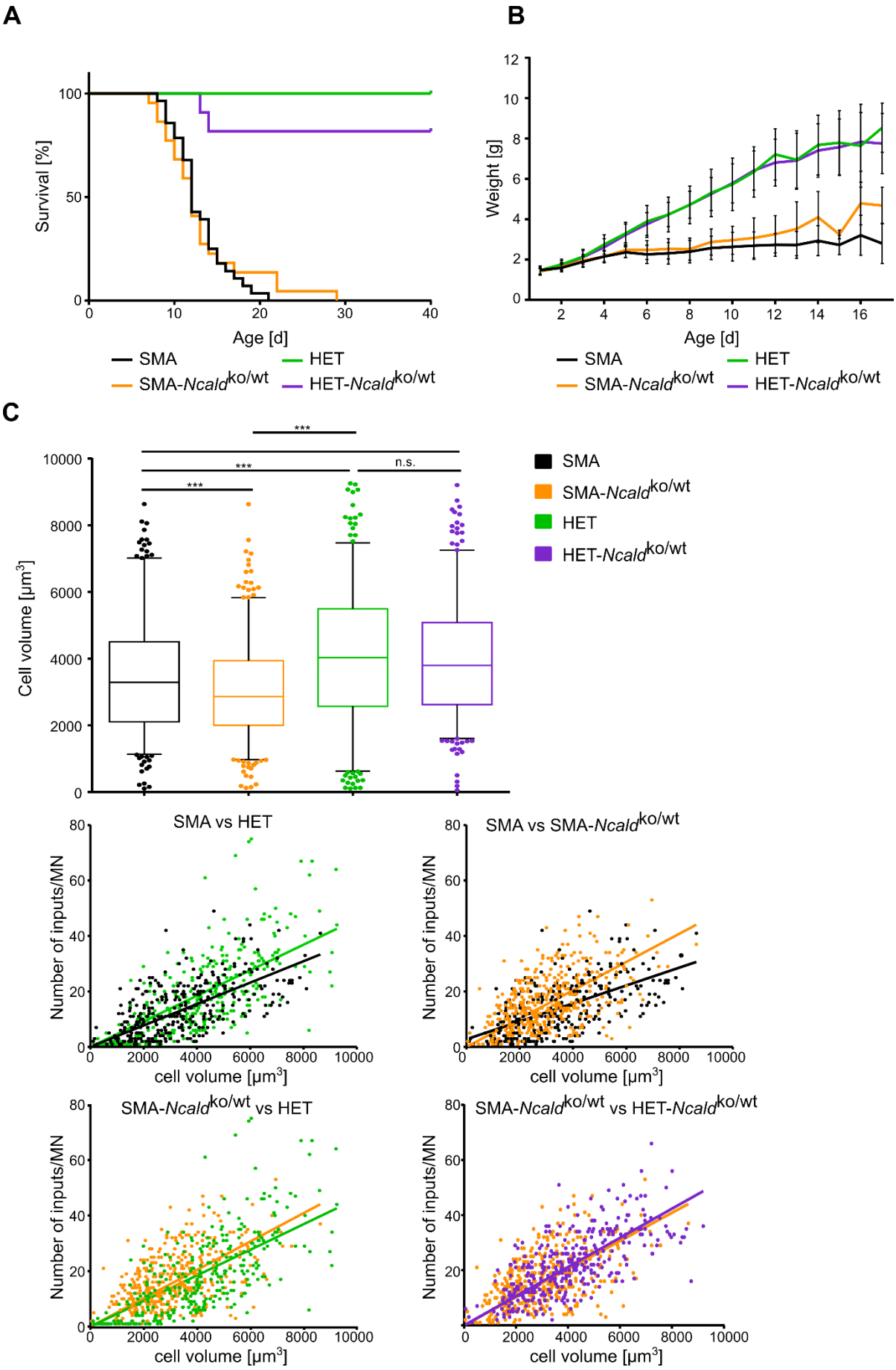
A
Survival [%]
Age [d]
SMA
SMA-Ncald ko/wt
HET
HET-Ncald ko/wt
B
Weight [g]
Age [d]
C
Cell volume [µm³]
***
n.s.
SMA vs HET
SMA vs SMA-Ncald ko/wt
SMA-Ncald ko/wt vs HET
SMA-Ncald ko/wt vs HET-Ncald ko/wt
Number of inputs/MN
cell volume [µm³]

**Figure S5. Characterization of Heterozygous *Ncald* Knockout in SMA Mice: Survival, Weight Progression and Proprioceptive Inputs on Motor Neurons: Heterozygous *Ncald* Knockout Ameliorates Input Number but not Cell Size.**

(A) Mean survival of SMA mice on pure C57BL/6N: SMA = 12.9±3.2 days, N = 28, SMA-*Ncald*$^{ko//wt}$ = 13.1±5.3 days, N = 22.

(B) The weight of SMA and SMA-*Ncald*$^{ko/wt}$ mice is reduced significantly from P5 onwards when compared to HET and HET-*Ncald*$^{ko/wt}$. Error bars indicate SD. N >20 for each genotype.

(C) The MN cell volume [µm$^3$] of SMA and SMA-*Ncald*$^{ko/wt}$ is significantly smaller in comparison to HET. Analysis of proprioceptive inputs on spinal MN relative to cell volume: individual values of input number were plotted against cell volume and linear regression was drawn. The number of proprioceptive inputs in SMA-*Ncald*$^{ko/wt}$ MN is increased independently of cell volume and input number/cell volume ratio was similar in SMA-*Ncald*$^{ko/wt}$ and HET-*Ncald*$^{ko/wt}$ MN. N = 3/genotype, n = 100-120 MN/animal. ***P < 0.001. Box plots defined in Figure 4.

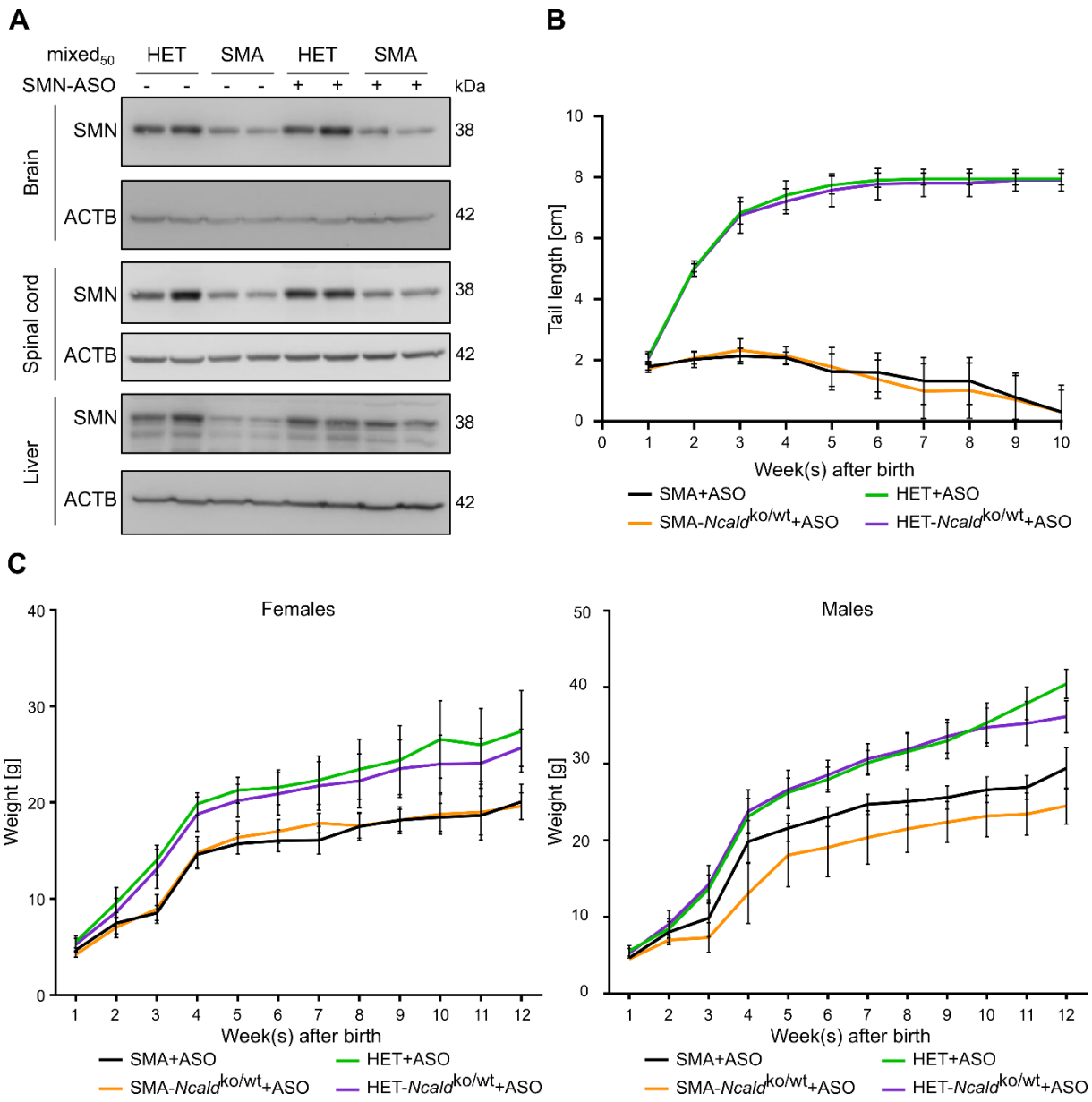


**Figure S6 SMN-ASO Functionality Testing, Tail Length and Weight Progression in the SMA+ASO Mouse Model**

(A) Western blot of spinal cord, brain and liver lysates of P4-old control-ASO or SMN-ASO injected mixed$_{50}$ HET or SMA mice. SMN levels were increased in the liver, but not in the brain or spinal cord after SMN-ASO injection. Beta-Actin (ACTB) was used as loading control.

(B) Tail length of SMN-ASO injected mixed$_{50}$ mice was measured weekly; tail necrosis in SMA+ASO (N = 7) and SMA-*Ncald*$^{ko/wt}$+ASO (N = 9) mice started between the 6$^{th}$ and 8$^{th}$ week after birth. Control mice: HET+ASO (N = 9); HET-*Ncald*$^{ko/wt}$+ASO (N = 10). Error bars indicate SD.

(C) Weight of female (F) and male (M) of SMN-ASO injected mixed$_{50}$ mice was measured weekly. SMA+ASO (F = 7, M = 5), SMA-*Ncald*$^{ko/wt}$+ASO (F = 4, M = 9), HET+ASO (F = 7, M = 9), HET-*Ncald*$^{ko/wt}$+ASO (F = 8, M = 9). Error bars indicate SD.

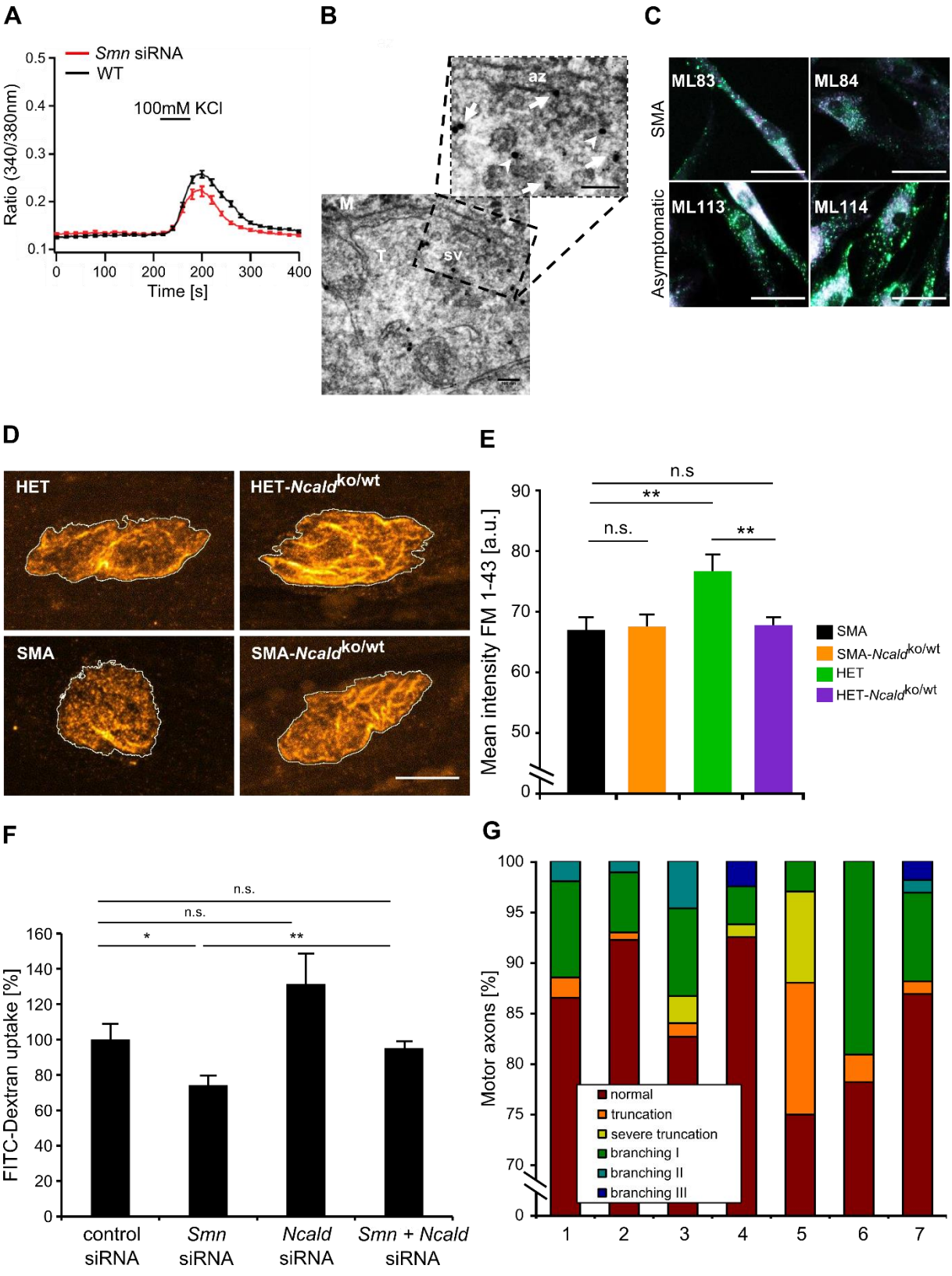
A
Smn siRNA
WT
100mM KCl
Ratio (340/380nm)
Time [s]
B
az
M
T
sv
C
SMA
Asymptomatic
ML83
ML84
ML113
ML114
D
HET
HET-Ncald ko/wt
SMA
SMA-Ncald ko/wt
E
Mean intensity FM 1-43 [a.u.]
n.s
**
n.s.
**
SMA
SMA-Ncald ko/wt
HET
HET-Ncald ko/wt
F
FITC-Dextran uptake [%]
n.s.
n.s.
*
**
control siRNA
Smn siRNA
Ncald siRNA
Smn + Ncald siRNA
G
Motor axons [%]
normal
truncation
severe truncation
branching I
branching II
branching III

**Figure S7 Voltage Induced $Ca^{2+}$ Dynamics of Cells Treated with *Smn* siRNA or *Smn+Ncald* siRNA; Impact of $Ca^{2+}$ on Endocytosis**

(A) Ratiometric $Ca^{2+}$ imaging with fura-2 in differentiated PC12 cells showed that the increase in cytosolic $Ca^{2+}$, which is triggered by KCl-induced, is reduced in SMN depleted cells (N = 3, n = 41) compared to control cells (N = 3, n = 38); P<0.001.

(B) Immunogold staining of NMJs of 48 hpf control zebrafish embryos. Ncald is visualized by secondary antibody labelled with 20 nm gold particle (big black dots) and clathrin with 6 nm gold particle (small black dots). Ncald (white arrows) is localized to synaptic vesicles and the active zone (az) of the presynapse and clathrin is localized to some synaptic vesicles (black arrows); white arrowheads mark the colocalization of Ncald and clathrin at synaptic vesicles. M = muscle fiber, T = nerve terminal, scale bar, 100 nm.

(C) Representative images of fibroblasts derived from Utah family members, SMA patients and controls after endocytosis assay. After starvation cells were incubated for 20 min with FITC-dextran (green), fixed and counterstained with phalloidin-AlexaFluor 568 (red). The FITC signal is higher in asymptomatic cells. Scale bar, 50 µm. For quantification see also Figure 5C.

(D) Representative images of endocytic FM1-43 uptake at the presynaptic terminals on P10 in TVA muscles under low frequency stimulation (5 Hz, 1s). Postsynaptic receptors staining (BTX-Alexa647) was used to define the area to analyze the FM1-43 uptake (orange) at the presynaptic terminals. Scale bar, 10 µm. For quantification see also Figure 5D.

(E) Quantification of the FM1-43 mean intensity at the presynaptic terminals on P10 in TVA muscles under high frequency stimulation (20 Hz, 1s). For each genotype 3 animals and ~100 NMJs were analysed. Error bars represent SEM. n.s. non-significant; ***P <0.001.

(F) FACS-based quantification of FITC signal in NSC34 cells treated with respective siRNA. *Ncald* KD resulted in elevated FITC-dextran endocytosis. *Smn* KD decreased endocytosis (*P <0.05), which was fully restored by additional *Ncald* KD (*Smn* siRNA vs. *Smn+Ncald* siRNA: **P <0.01 control siRNA vs. *Smn+Ncald* siRNA: n.s.). N=6 biological replicates per siRNA treatment, individual sample n=50.000 cells.

(G) Quantitative analysis of motor axon phenotype of 34 hpf zebrafish, subjected to the respective treatment: 1 = *ncald* MO (2 ng), 2 = *smn+ncald* MO (2 ng), 3 = *ncald* MO + Pitstop2 (12.5 µM), 4 = control + Pitstop2 (25 µM), 5 = *smn* MO + Pitstop2 (25 µM), 6 = *smn* MO+*ncald* MO + Pitstop2 (25 µM), 7 = *ncald* MO + Dynasore (25 µM). Note the rescue effect of *ncald* MO injection on the truncation phenotype of *smn* MO and 25 µM Pitstop2 treated zebrafish (bars 5 and 6).

**SUPPLEMENTAL TABLE**

**Table S1** Human fibroblast and EBV-transformed lymphoblastoid cell lines (LBs) derived from SMA patients, carriers and asymptomatic individuals used in this work.

| **Phenotype Utah Family** | **ID-No** | ***SMN1*/*SMN2*** | **DNA#** | **Fibroblast #** | **LB#** |
|---|---|---|---|---|---|
| | | | | | |
| SMA type I | IV-5 | 0/2 | 9994 | ML83 | B9994 |
| SMA type I | IV-2 | 0/2 | 9164 | ML84 | B9164 |
| asymptomatic | IV-4 | 0/4 | 9120 | ML113 | B9120 |
| asymptomatic | IV-3 | 0/4 | 9119 | ML114 | B9119 |
| asymptomatic | III-1 | 0/4 | 9128 | ML115 | B9128 |
| asymptomatic | III-4 | 0/4 | 9124 | ML117 | B9124 |
| asymptomatic | III-6 | 0/4 | 9126 | ML118 | B9126 |
| carrier | II-1 | 1/3 | 9129 | ML146 | B9129 |
| carrier | III-2 | 1/1 | 9122 | | B9122 |
| carrier | III-3 | 1/1 | 9123 | | B9123 |
| carrier | III-5 | 1/4 | 9125 | | B9125 |
| carrier | III-7 | 1/4 | 9127 | | B9127 |
| carrier | I-2 | 1/4 | 9133 | | B9133 |
| carrier | III-8 | 1/2 | 9165 | | B9165 |
| carrier | IV-1 | 1/2 | 9118 | | B9118 |
| carrier | II-4 | 1/2 | 9132 | | B9132 |
| non-carrier | I-1 | 2/0 | 9134 | | B9134 |
| **Independent SMA patients** | | | | | |
| SMA type III | | 0/3 | 326 | | BW70 |
| SMA type II | | 0/4 | 798 | | BW174 |
| SMA type II | | 0/4 | 1086 | | BW214 |
| SMA type III | | 0/4 | 2349 | | BW303 |
| SMA type III | | 0/4 | 1141 | | BW232 |
| SMA type II | | 0/4 | 146 | | T110/91 |
| SMA type III | | 0/4 | 906 | | BW184 |
| SMA type III | | 0/4 | 106 | | T77/91 |
| SMA type III | | 0/4 | 530 | | BW145 |
| SMA type III | | 0/5 | 6241 | | LN498 |
| SMA type III | | 0/4 | 6981f | ML69 | |
| SMA type I | | 0/2 | 3413 | ML17 | |
| SMA type III | | 0/3 | 2027 | ML12 | BW332 |
| SMA type I | | 0/3 | 4043 | ML16 | |
| SMA type III | | 0/3 | 2026 | ML14 | BW333 |
| SMA type III | | 0/4 | 11268c | ML106 | |
| SMA type II | | 0/3 | 785 | ML5 | |
| SMA type I | | 0/2 | 4814b | ML39 | |
| control | | | | ML32 | |
| control | | | | ML35 | |
| control | | | | ML44 | |

## SUPPLEMENTAL REFERENCES

Swoboda, K.J., Prior, T.W., Scott, C.B., McNaught, T.P., Wride, M.C., Reyna, S.P., and Bromberg, M.B. (2005). Natural history of denervation in SMA: relation to age, SMN2 copy number, and function. Ann Neurol *57*, 704-712.